UNIVERSITY OF THESSALY
SCHOOL OF ENGINEERING
DEPARTMENT OF MECHANICAL ENGINEERING
LABORATORY OF ALTERNATIVE ENERGY CONVERSION SYSTEMS

THESIS

FABRICATION AND CHARACTERIZATION OF ELECTROCHEMICAL AMMONIA SENSORS

By: **ANTONIOS VOUZAVALIS**
STERGIOS GEORGANTAS

Submitted in fulfillment of the requirements for the Diploma in the Department of Mechanical Engineering of the University of Thessaly

Volos, 2017

Εγκρίθηκε από τα Μέλη της Τριμελούς Εξεταστικής Επιτροπής:

Examiner: (Supervisor)
Dr Tsiakaras Panagiotis
Professor of Department of Mechanical Engineering,
School of Engineering
University of Thessaly

Examiner:
Dr Stapountzis Herricos
Professor of Department of Mechanical Engineering,
School of Engineering
University of Thessaly

Examiner:
Dr Brouzgou Angeliki
Senior Researcher and Teaching Staff of
Department of Mechanical Engineering,
School of Engineering
University of Thessaly

ABSTRACT

Due to the extensive use of ammonia in a wide range of industrial sectors and the high risk that derives from a leakage possibility, smart, cheap and flexible devices need to be developed for ammonia monitoring. For this purpose, the scientific community emphasizes on developing electrochemical sensors, which seem to have a promising potential. In the present work, a review on electrochemical gas sensors is presented as well as a proposal for a novel ammonia electrochemical sensor alongside with experimental data.

At first, the basic theory of electrochemistry and diffusion is examined, which is essential for the function of electrochemical sensors. An overview of the most common commercial electrochemical devices is displayed, with emphasis on electrochemical sensors.

The classification and operation principles of various gas sensors is analyzed, with a further analysis on high and intermediate operating temperature. The configuration, the I-V curves and the applications of each sensor is presented.

In the end, a novel ammonia electrochemical sensor is proposed. This amperometric sensor based on oxygen ion solid electrolyte for the measurement of ammonia was fabricated and tested. The architecture and operational features of this sensor based on $0.91ZrO_2+0.09Y_2O_3$ solid electrolyte for the detection of 1-5 vol. % NH_3 in N_2 at a temperature range of 375-400^oC is described. The values of the ammonia's diffusion coefficient in nitrogen, at elevated temperatures can also be obtained.

ΠΕΡΙΛΗΨΗ

Εξαιτίας, της εκτεταμένης χρήσης της αμμωνίας σε ένα μεγάλο εύρος βιομηχανικών τομέων καθώς και του υψηλού κινδύνου που εγκυμονεί σε περίπτωση διαρροής, είναι αναγκαία η ανάπτυξη έξυπνων, φθηνών και ευέλικτων συσκευών για τον έλεγχό της. Για το σκοπό αυτό, η επιστημονική κοινότητα δίνει έμφαση στην ανάπτυξη ηλεκτροχημικών αισθητήρες, οι οποίοι παρουσιάζουν πολλά υποσχόμενες προοπτικές. Στην παρούσα εργασία, πραγματοποιείται μια σύνοψη στους ηλεκτροχημικούς αισθητήρες αερίων, καθώς επίσης και μία πρόταση για έναν καινοτόμο ηλεκτροχημικό αισθητήρα αμμωνίας, η οποία συνοδεύεται από τα πειραματικά αποτελέσματα.

Αρχικά, εξετάζεται η βασική θεωρία της ηλεκτροχημείας και της διάχυσης, οι οποίες είναι απαραίτητες για τη λειτουργία των ηλεκτροχημικών αισθητήρων. Παρουσιάζεται μια ανασκόπηση των πιο κοινών εμπορικών ηλεκτροχημικών συσκευών με έμφαση στους αισθητήρες.

Αναλύεται η ταξινόμηση και η αρχή λειτουργίας διαφόρων αισθήτηρων αερίων με μια περαιτέρω ανάλυση σε αισθητήρες υψηλής και ενδιάμεσης θερμοκρασίας λειτουργίας. Η διάταξη, τα διαγράμματα I-V και οι εφαρμογές του κάθε αισθητήρα περιγράφονται επίσης.

Τέλος, προτείνεται ένας νέος ηλεκτροχημικός αισθητήρας αμμωνίας. Κατασκευάστηκε και δοκιμάστε ο συγκεκριμένος αμπερομετρικός αισθητήρας βασισμένος σε στερεό ηλεκτρολύτη ιόντων οξυγόνου για τη μέτρηση της αμμωνίας. Περιγράφεται η κατασκευή και τα λειτουργικά χαρακτηριστικά του αισθητήρα, ο οποίο βασίζεται στο στερεό ηλεκτρολύτη $0.91ZrO_2+0.09Y_2O_3$, για την ανίχνευση 1-5 vol.% NH_3 σε N_2 σε εύρος θερμοκρασίας 375-400 ^oC. Είναι επίσης δυνατή η εύρεση των τιμών του συντελεστή διάχυσης της αμμωνίας σε άζωτο, σε αυξημένες θερμοκρασίες.

ACKNOWLEDGEMENTS

We would like to express our great and sincere gratitude to our supervisor, Professor Panagiotis Tsiakaras, for his commitment, advice, guidance, immense interest, knowledge, patience and support. We would also like to thank him for accepting us to study and work at the Laboratory of Alternative Energy Conversion Systems at the Department of Mechanical Engineering in University of Thessaly, where the experimental work was made.

The completion of the present work would not have been possible without the support and encouragement of Dr Sotiria Kontou and Dr Angeliki Brouzgou. Their patience as well as their assistance and guidance in both the theoretical and experimental part of our work was of great importance. Furthermore we feel the necessity to thank the members of the examination committee, Dr Angeliki Brouzgou and Professor Herricos Stapountzis, for their time and useful advice.

Moreover, we are grateful to our friends Mr. Nikos Malamas and Mr. Stavros Katsaros, with whom we had the pleasure and luck to work and cooperate with. We express our sincere gratitude to graphic designer Ioanna Manoli too, for editing front and back cover.

Also, we would like to thank our families for their love and the moral and financial support that they provided not only during the composition of the present work, but throughout our studies at the Department of Mechanical Engineering in University of Thessaly.

Antonios Vouzavalis
Stergios Georgantas

ΕΥΧΑΡΙΣΤΙΕΣ

Θα θέλαμε να εκφράσουμε τη μεγάλη και ειλικρινή μας ευγνωμοσύνη στον υπεύθυνο καθηγητή μας κ. Παναγιώτη Τσιακάρα για την αφοσίωση, καθοδήγηση, καθώς και το τεράστιο ενδιαφέρον, γνώση και υποστήριξη που υπέδειξε. Θα θέλαμε επίσης να τον ευχαριστήσουμε που μας δέχτηκε στο Εργαστήριο Εναλλακτικών Συστημάτων Μετατροπής Ενέργειας του Τμήματος Μηχανολόγων Μηχανικών του Πανεπιστημίου Θεσσαλίας, όπου και πραγματοποιήθηκε το πειραματικό κομμάτι της εργασίας.

Η ολοκλήρωση της παρούσας εργασίας δε θα ήταν δυνατή χωρίς την υποστήριξη και ενθάρρυνση των Δρ Σωτηρίας Κόντου και Δρ Αγγελικής Μπρούζγου. Η υπομονή τους καθώς επίσης η βοήθεια και καθοδήγησή τους στο θεωρητικό και πειραματικό μέρος της εργασίας ήταν καθοριστική. Ακόμα, οφείλουμε ένα μεγάλο ευχαριστώ στα μέλη της εξεταστικής επιτροπής, Δρ Αγγελική Μπρούζγου και καθηγητή κ. Ερρίκο Σταπουντζή, για το χρόνο τους και τις χρήσιμες συμβουλές τους.

Επίσης, είμαστε ευγνώμονες στους φίλους μας κ. Νίκο Μαλαμά και κ. Σταύρο Κατσαρό, με τους οποίους είχαμε τη χαρά να δουλέψουμε και να συνεργαστούμε. Ακόμα θα θέλαμε να εκφράσουμε την ειλικρινή μας ευγνωμοσύνη στη γραφίστα Ιωάννα Μανώλη για την επιμέλεια του εξώφυλλου και του οπισθόφυλλου.

Τέλος, θα θέλαμε να ευχαριστήσουμε τις οικογένειές μας για την αγάπη τους και την ηθική και οικονομική υποστήριξη που παρείχαν όχι μόνο κατά την εκπόνηση της παρούσας εργασίας αλλά και κατά τη διάρκεια των σπουδών μας στο Τμήμα Μηχανολόγων Μηχανικών του Πανεπιστημίου Θεσσαλίας.

Αντώνιος Βουζάβαλης
Στέργιος Γεωργαντάς

CONTENTS

LIST OF TABLES

LIST OF FIGURES

CHAPTER 1: INTRODUCTION

Abstract

In the present chapter, the utility of ammonia in industry and other sectors is presented. Ammonia danger awareness is taken under consideration as well as the necessity for developing smart and flexible ammonia monitoring devices. Moreover, the history of electrochemical devices is briefly introduced.

1.1 Utility of ammonia in industry

Ammonia is a very important industrial chemical, and is used widely in both its pure form and as a feedstock for a wide variety of other chemicals. Agricultural industries are the major users of ammonia, because it is a valuable source of nitrogen that is essential for the growth of plants. Ammonia is also used in the production of liquid fertilizer solutions, which consist of ammonia, ammonium nitrate, urea and aqua ammonia. Apart from the agricultural and fertilizer industry, it is valuable in industrial refrigeration systems, rubber and petroleum industry and metal treating operations. A smaller amount of ammonia is also used in chemical laboratories for research purposes.

Nearly 85% of the amount of ammonia that is produced, is utilized in the agricultural industry. The fast development of this industrial sector, alongside with the general industrial development over the last years, has led to a significant increase in the annual generation of ammonia. It is, therefore, obvious, that ammonia is a chemical compound of great significance in the industrial operation, and a further growth in its production is expected over the next years.

1.2 Danger awareness and monitoring

Apart from the benefits that provides, the extensive use of large amounts of ammonia can be dangerous. Ammonia gas is lighter than air and will rise. In the presence of moisture, ammonia can form vapors that are heavier than air. These vapors can spread along the ground or other low-lying areas.

Ammonia is a colorless gas that is characterized by an intense and unpleasant odor. It can enter the human body through the respiratory system. Due to its basic nature, it cause a burning feeling in the eyes, respiratory tract and the skin. The severity of the damage depends on the concentration and the period of exposure. Exposure to large amounts can even cause death. Consequently, precautionary measures and frequent checking for leakages are crucial both in the industrial and in the laboratory sector as well.

For achieving the desirable quality of production and/or prevention of dangerous situations, monitoring of ammonia during various technological processes is required. It is perceived, that due to the extensive use of ammonia, the development of smart, low-cost and flexible monitoring devices is essential.

The deployment of electrochemical gas sensors is presented as a promising and solution, which meet the aforementioned expectations. Their operation principle is similar to those of all the electrochemical devices.

1.3 History of electrochemical devices

The first battery was invented by Alessandro Volta in 1800. He constructed a pile that consisted of zinc and silver discs separated by a piece of cardboard that had been soaked in saltwater. A wire connecting the bottom zinc disc to the top silver disc could produce repeated sparks. Later, Volta showed that any pair of different metals could be used for the construction of such a pile [1].

Another battery cell that became popular during the 19th century was invented in 1836 by the English chemical John Frederick Daniell. Zinc and copper were used for this cell; the basic principle was the same with Volta's pile, with the difference that each metal was surrounded by its metallic ion solution and that the solutions were kept separated by a porous ceramic septum. Each metal with its solution constituted a half-cell. A zinc half-cell and a copper half-cell formed a voltaic cell. This configuration created a primary form of electrochemical cells, which presumed upon the spontaneous reaction to produce energy [1]:

$$Zn(s) + Cu^{2+}(aq) \rightarrow Zn^{2+}(aq) + Cu(s) \qquad (1.1)$$

In 1800, the water electrolysis process was described by William Nicholson and Anthony Carlisle. William Grove, in 1839, accomplished "water recomposition" with a device called a "gas battery". Its operation was based on two Pt electrodes in oxygen and hydrogen gas. One end of each electrode was immersed in a container of sulfuric acid. Water was held at the container as well and it was observed that the water level rose in both tubes as current flowed. This configuration was the precursor of the Grove cell which consisted of a platinum and a zinc electrode immersed in nitric acid and zinc sulfate respectively; it generated 12A of current at 1.8V. This was the first known demonstration of the fuel cell [2].

The first electrochemical sensors appeared in 1930s. However, no further development was made until the 1950s, when some of the most important sensors was constructed. In 1956, Clark invented an oxygen sensor based on a Pt electrode and the first biosensors in the 1962, with Lyons. Only after the 1970s and 1980s noteworthy progress in electrochemical sensors was achieved [3].

The electrochemical devices that have been formed since then base their working principle on the primitive designs that were deployed in the beginning of the 20^{th} century.

CHAPTER 2: ELECTROCHEMICAL CELL

Abstract

In the present chapter the structure, configuration and basic parts of the electrochemical cell are presented. The function of each compartment of the cell and its operating principle is described as well.

2.1 Configuration and principle of operation

A voltaic cell consists of two half-cells, which are electrically connected with each other. A half-cell is the part of the electrochemical cell where a half-reaction takes place [1].

The electrochemical cell is the heart of the electrochemical device. Its basic format consists of two electrodes, an anode and a cathode, and an electrolyte that separates them. Apart from that, the device also consists of interconnects, sealings and a distribution system for the fuel. The material selection for each component is based on its operating requirements and properties as well as its working temperature.

The anode is the electrode where the oxidation of the fuel occurs. The electrons produced in the oxidation reaction flow through an external circuit to the cathode side. The most important properties of the anode are good electronic conductivity, good electro-catalytic activity to facilitate the reaction and good microstructural strength to operate in high temperatures, depending on the type of the device [4].

The reduction reaction takes place at the cathode. The desirable properties of the cathode are high electronic and ion conductivity, chemical stability at operating temperatures and a better catalyst for the reduction reaction, which is the rate-limiting step for the device's efficiency [4].

The electrolyte is a membrane that divides the anode and the cathode. Its purpose is to allow ions to pass from the anode to the cathode. The electrolytes are separated based on their state into liquid and solid. Typical liquid electrolytes are alkali, molten carbonate and phosphoric acid, while some of the solid electrolytes are solid oxide, and proton exchange membranes (PEM). Furthermore they are categorized by the type of ion that is transported through the electrolyte. For example, there are oxygen ion electrolytes (Y_2O_3, CaO, and Yb_2O_3) and proton conducting electrolytes. The electrolytes have to meet several criteria such as good ionic conductivity at the operating temperatures and

thermodynamic and chemical stability in reducing and oxidizing environments. Also, they should be non-electron conductors, therefore they should be fully dense and leak-tight and endure high mechanical and thermal stress [4].

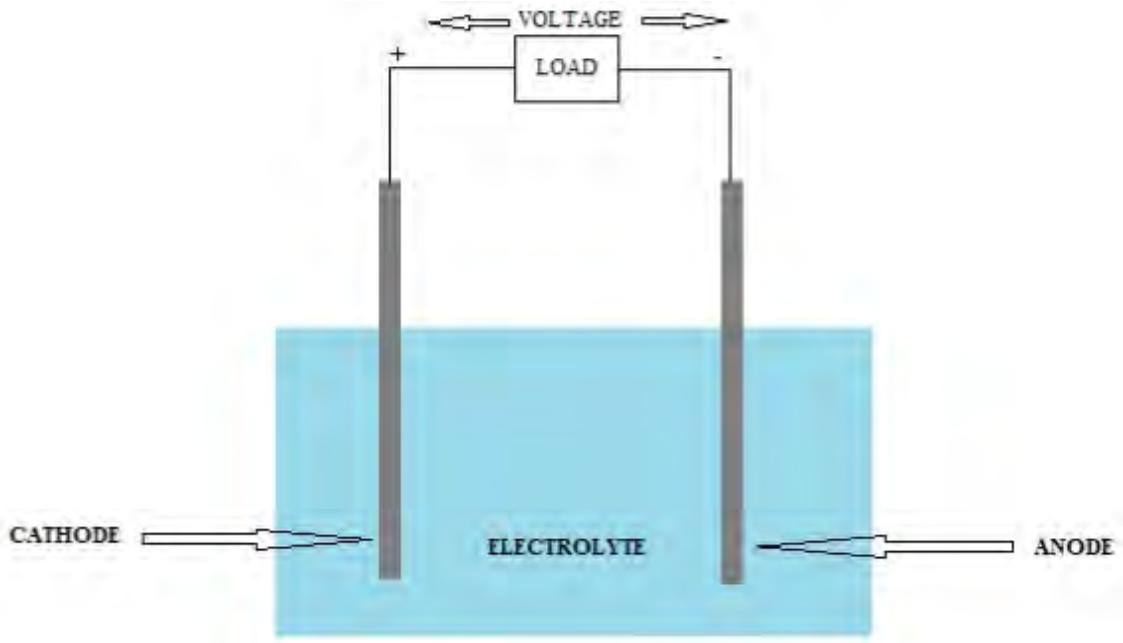

Figure 2.1. Components of an electrochemical cell.

The operation principle of the electrochemical cell is common for all the electrochemical devices. In every electrochemical cell a redox reaction takes place. Redox reaction are divided into 2 half-reactions, an oxidation and a reduction. Oxidation is the loss of electrons or an increase in oxidation state by a molecule, atom, or ion, while reduction is the gain of electrons or a decrease in oxidation state. The electrons which were gained by the oxidation are transferred through an external circuit to the other half cell, where the reduction reaction takes place. The electric transfer is divided into an electronic and an ionic charge transfer.

Oxidation

$$Reductant \rightarrow Ox.Product + e^-$$

Reduction

$$Oxidant + e^- \rightarrow Red.Product$$

Redox

$$Reductant + Oxidant \rightarrow Ox.Product + Red.Product$$

CHAPTER 3: BASIC ELECTROCHEMISTRY

Abstract

In this chapter, is an introduction to the electrochemistry fundamentals, which are necessary for a deeper understanding of the operation of electrochemical cells. More specifically, the concept of electromotive force, Nernst Equation, Butler-Volmer and Tafel Equations, Faraday's Law and the concept of limiting current are examined.

3.1 Electromotive Force and Nernst Equation

The work required for the movement of electric charge through a conductor depends on the amount of the charge that is moved and the potential difference. The potential difference is the difference in electric potential between two points and is measured in volts (V). During the operation of the electrochemical cell, the potential difference (voltage) between the electrodes is less than the maximum possible voltage of the cell. The decrease in the voltage of a cell occurs due to the flow of electric current and the energy that is required.

The voltage of the cell decreases as long as the amount of the electric current increases and consequently reaches its maximum value only when no current flows [5]. The maximum voltage of the cell is referred to as electromotive force (EMF), E_{cell} and it depends on the state of the cell, such as temperature, pressure and concentration. When the measurement takes place under standard states - concentration 1M, temperature 25^{o}C, pressure 1 atm – the cell voltage is referred to as the standard state cell potential E^{o}_{cell}. The cell potential is calculated by the sum of the half-cell potential of the reduction and the oxidation:

$$E_{cell} = E_{reduction} + E_{oxidation}$$

or

$$E_{cell} = E_{cathode} + E_{anode}$$

Gibbs energy, ΔG, is the difference in the energy between the reactants and products of a reaction. For an electrochemical cell, $\Delta G = -nFE_{cell}$, where n is the number of the transferred electrons during the reaction and F is the Faraday constant, which is the

amount of electric charge that is possessed by a mole of electrons. It equals 9.65×10^4 C. Under standard conditions, $\Delta G^o = -nFE^o_{cell}$.

The Nernst equation relates the potential generated by an electrochemical cell to the activities of the chemical species that take part in the reaction of the cell and to the standard potential, E^o [6]. It equals:

$$E = E^o - \frac{RT}{nF} ln\left(\frac{[Red]}{[Ox]}\right) \quad (3.1)$$

Where R=8.314 J/Kmol is the gas constant, T is the temperature in which the reaction occurs, F is the Faraday constant, n is the number of the transferred electrons and [Red] and [Ox] are the concentrations of the reductant and the oxidant that take place in the reaction, respectively.

3.2 Butler-Volmer and Tafel Equation

A non-spontaneous cell reaction occurs when an overpotential, η (V), is applied, $\eta = E - E_{cell}$, where E_{cell} is the EMF and E is the potential at which the redox event is experimentally observed.

The overpotential can be related with the rate of a reaction with the Butler-Volmer equation:

$$i = i_o \left[exp\left(\frac{\alpha_\alpha nF}{RT}\eta\right) - exp\left(\frac{\alpha_c nF}{RT}\eta\right)\right] \quad (3.2)$$

The 2 terms of eq. 3 express the rate of the anodic and cathodic direction, respectively.

$$i_\alpha = i_o \left[exp\left(\frac{\alpha_\alpha nF}{RT}\eta\right)\right] \quad (3.3)$$

$$i_c = i_o \left[exp\left(\frac{\alpha_c nF}{RT}\eta\right)\right] \quad (3.4)$$

The difference between these rates, $i = i_\alpha - i_c$, gives the net rate of the reaction. The parameter i_o is called the exchange current density. High exchange current density means that the redox reaction occurs rapidly in both directions. The sign of the overpotential determines the net direction of the redox reaction. n is the number of transferred electrons, while the parameters α_α and α_c are called anodic and cathodic transfer coefficients respectively and relate how an applied potential favors one direction of reaction over the other [7]. They are not independent variables; in general, $\alpha_\alpha + \alpha_c = 1$ and for many reactions $\alpha_\alpha + \alpha_c = 0.5$.

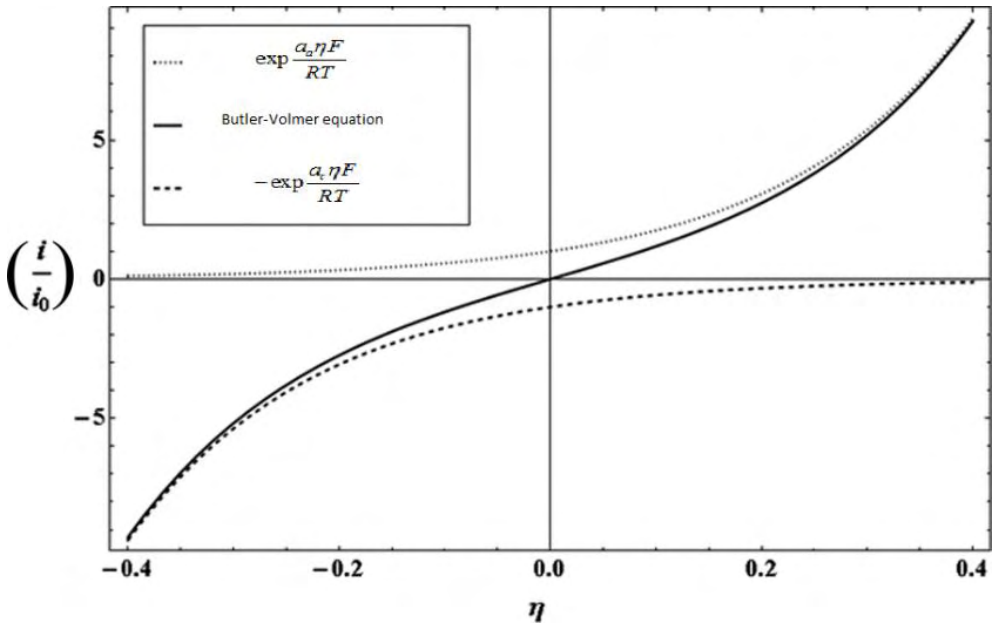

Figure3.1. Butler-Volmer equation plot [8].

When overpotential, η, receives highly negative values, cathodic current density increases while anodic current density becomes negligible. Therefore, the term (3.3) of the Butler-Volmer equation becomes negligible. Similarly, when the overpotential is highly positive, the term (3.4) of the Butler-Volmer reaction becomes negligible and anodic current density increases [9].

As it is shown in Fig. 3.1, for small values of η, the current density varies linearly. For high values of η (over 50mV) the increase in current is exponential with overpotential and the equation (3.4) can be also expressed as:

$$\log(-I_c) = \log I_o - \frac{\alpha_c nF\eta}{2.303RT} \qquad (3.5)$$

or in a simplified way:

$$\text{Reduction slope} = \frac{-a_c nF}{2.303RT} \qquad (3.6)$$

where 2.303 is the conversion from natural to decimal logarithm.

Similarly, when η receives highly positive values, anodic current density increases and cathodic current density becomes negligible and the term (3.4) as well. In this case, equation (3.3) is also expressed as:

$$\log I_\alpha = \log I_O + \frac{a_a nF\eta}{2.303RT} \qquad (3.7)$$

or

$$\text{Oxidation slope} = \frac{-\alpha_\alpha nF}{2.303RT} \qquad (3.8)$$

Equations (3.5) and (3.7) are called cathodic and anodic Tafel equations respectively. The slope of the linear region on the Tafel plot can be used to calculate the transfer coefficient α [9],[10].

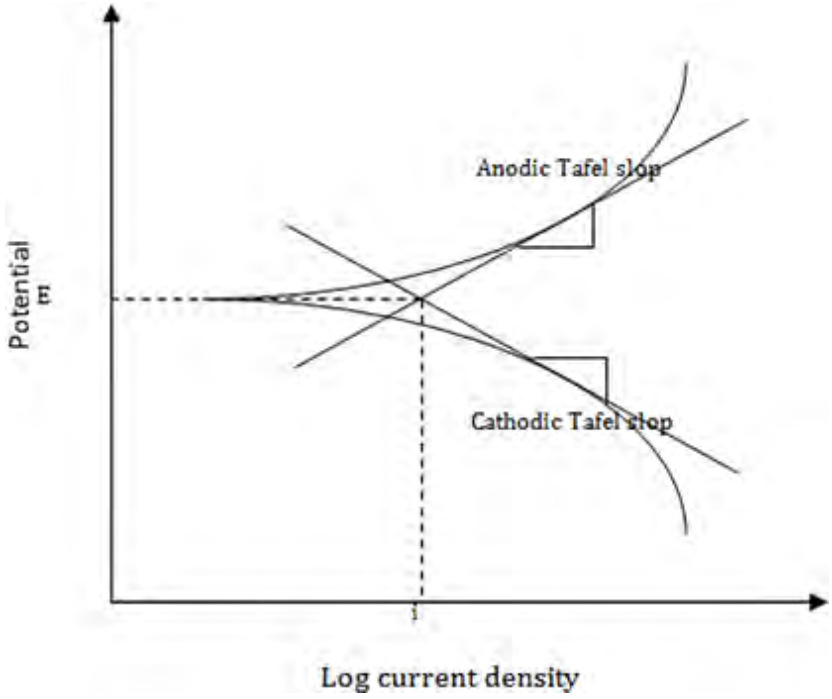

Figure 3.2. Tafel equation plot [11].

3.3 Faraday's Law

Faraday's law relates the total charge Q (C) that passes through an electrochemical cell to the amount of product N (mol):

$$Q=nFN \qquad (3.9)$$

where F is Faraday's constant and n is the number of electrons transferred per mole of product. Faraday's law can be used to find the amount of substance deposited at an electrode and even for the total amount of electricity required for complete electrolysis of a compound. The number of electrons implicated in an electrolytic process can be also found by the Faraday's law. For example, in a molten salt with the following reaction:

$$Al^{+++} + 3e^{-} \rightarrow Al \qquad (3.10)$$

the amount of aluminum produced is proportional to the number of electrons involved [12],[13].

3.4 Limiting Current

During a redox reaction, it is found that increasing the applied potential, a steep rise of the current is observed until it reaches a "plateau", indicating that the current value is stabilized regardless of further applied voltage. The current will rise again only when the potential receives much greater values.

The current plateau indicates that a particular electrode reaction proceeds at the highest possible rate. Limiting current describes the maximum rate at 100% current efficiency, at which this reaction can proceed in the steady state.

The occurrence of the limiting current indicates the slowness of transport of charged or uncharged species (ions and molecules respectively) through the solution. These species are consumed in the electrode reaction. Limiting current density is observed when the supply of a transferred species to the electrode surface is a rate-limiting factor [14].

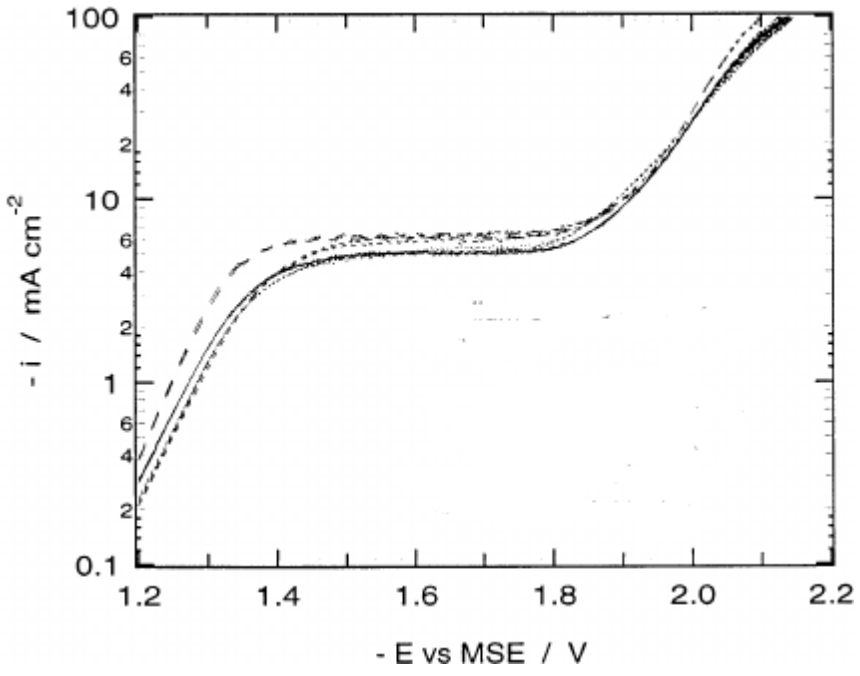

Figure 3.3. Linear potential sweep curves. The limiting current area is observed at ca. 1.4-1.8V [15].

CHAPTER 4: DIFFUSION

Abstract

In the present chapter, the fundamentals of diffusion regarding electrochemical devices are described. Molecular diffusion and Fick's Law are introduced, followed by Chapman-Enskog theory for binary diffusivity. The basic theory of Knudsen diffusion in porous media is also reviewed.

4.1 Introduction

Diffusion is the net movement of molecules or atoms from a region of high concentration (or high chemical potential) to a region of low concentration (or low chemical potential). This is also referred to as the movement of a substance down a concentration gradient. In electrochemical sensors, the magnitude of the current is controlled by how much of the target gas is oxidized at the working electrode. Sensors are usually designed so that the gas supply is limited by diffusion and thus the output from the sensor is linearly proportional to the gas concentration.

Gas diffusion has been thoroughly studied and there are mechanisms, depending on the characteristic of the diffusing gas species and the intrinsic microstructure of the porous media. Molecular diffusion or continuum diffusion refers to the relative motion of different gas species. The mean free path of gas molecules is at least one order larger than the pore diameter of the porous media. In Knudsen diffusion, the mean free path of gas molecules is on the same order as the tube dimensions.

Each mechanism is identified by the Knudsen number (K_n), which is the ratio of the gas mean free path to the pore size of the electrode:

$$K_n = \frac{\lambda}{d_p} \qquad (4.1)$$

where d_p is the diameter of the pores and λ is the gas mean free path, which is calculated by:

$$\lambda = \frac{k_B T}{\sqrt{2} p \pi d_g^2} \qquad (4.2)$$

where p is the gas pressure, d_g is the effective diameter of a gas molecule, k_B is the Boltzmann constant and T is the temperature of the gas (K).

If $K_n>>10$, collisions between gas molecules and the porous electrode are more dominant than the collisions between gas molecules. As a result, molecular diffusion is negligible. On the other hand, if $K_n<<0.1$, collisions and interactions between gas molecules become dominant and Knudsen diffusion becomes negligible compared with molecular and viscous diffusion. If $0.1<K_n<10$, all three mechanism participate in gas diffusion.

4.2 Molecular Diffusion

The most popular mathematical model for molecular diffusion in clear gases and fluids is Fick's law. Fick's first law describes the correlation between the diffusion flux of a gas component and the concentration gradient under steady-state conditions.

$$J_i = \frac{-D_i}{RT}\frac{c_i \partial(\mu_i)}{\partial x} \qquad (i=1,2,\ldots,n) \qquad (4.3)$$

Where J_i is the flux of gas species i, D_i is the bulk diffusivity, R is the gas constant, T is temperature, x is one-dimensional diffusion path, c_i is molar fraction of gas species i, and μ_i is the chemical potential of species i at a given state. μ_i can be expressed by:

$$\mu_i = \mu_0 + RTln(c_i) \qquad (4.4)$$

For application in porous media, Fick's first law is modified by the introduction of porous media factors:

$$D_{ij}^{eff} = \frac{\varphi}{\tau} D_{ij} \qquad (4.5)$$

Where D_{ij} is the binary diffusivity of gas species 1 and 2. D_{ij}^{eff} is the effective binary diffusivity of gas species 1 and 2, and φ and τ are the porosity and tortuosity of the porous media respectively.

The binary diffusivity D_{ij} can be calculated from the Chapman-Enskog theory:

$$D_{ij} = \frac{0.00186T^{\frac{3}{2}}}{p\sigma_{ij}^2\Omega}\left(\frac{1}{M_i}+\frac{1}{M_j}\right)^{\frac{1}{2}} \qquad (4.6)$$

Where D_{ij} is the diffusion coefficient measured in cm^2/s, T is the absolute temperature in K, p is the pressure in atm, and M_i are the molecular weights. σ_{ij} is the collision diameter given in angstroms and is calculated by:

$$\sigma_{ij} = \frac{1}{2}\left(\sigma_i + \sigma_j\right) \qquad (4.7)$$

Ω is a dimensionless quantity and its estimation depends on the integration of the interaction between the two species.

Fick's second law of diffusion also describes molecular diffusion, and more specifically predicts the effects of concentration change with time on diffusion mechanism:

$$\frac{\partial c_i}{\partial t} = D_i \frac{\partial^2 c_i}{\partial x^2} \qquad (4.8)$$

Since the study of electrochemical devices concerns continuous operation, we focus on Fick's first law.

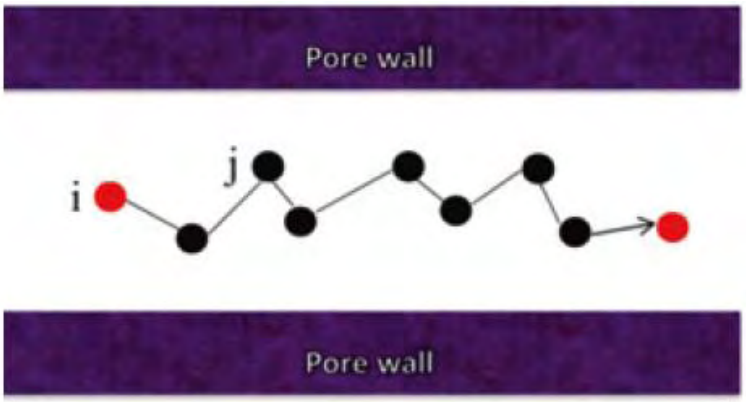

Figure 4.1. Illustration of pure molecular diffusion [16].

4.3 Knudsen diffusion

Due to the influence of walls, Knudsen diffusion is effected by the porous medium. The molecular flux of gas i due to Knudsen diffusion is given by the general diffusion equation:

$$J_{iK} = -D_{iK} \frac{\partial c_i}{\partial x} \qquad (4.9)$$

Where D_{Ik} is the Knudsen diffusivity, which is estimated from:

$$D_{iK} = \frac{d_p}{3} \sqrt{\frac{8RT}{\pi M_i}} \qquad (4.10)$$

Where M_i represents the molecular weights of gas species i, and d_p is the mean pore size of the porous media [17].

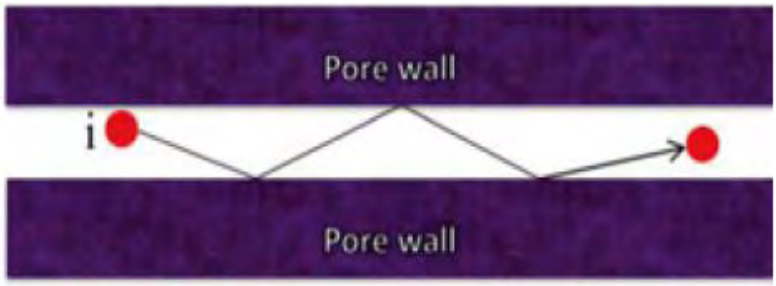

Figure 4.2. Illustration of pure Knudsen diffusion [16].

In general, the Knudsen model is important only at low pressures and small pore diameters. However, in many cases both Knudsen diffusion and molecular diffusion (D_{ij}) are of significance.

$$\frac{1}{D_i^t} \cong \frac{1}{D_{ij}} + \frac{1}{D_{iK}} \qquad (4.11)$$

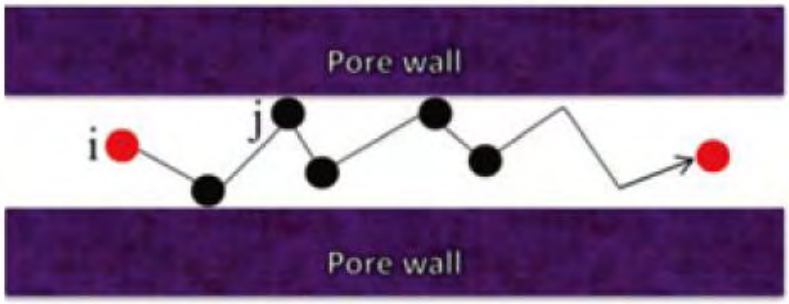

Figure 4.3. Illustration of Knudsen and molecular diffusion within straight cylindrical pores [16].

The above relationship refers to diffusion within straight and cylindrical pores, place in a parallel array. However, the most common configuration is that pores of various diameters are twisted and interconnected with one another. In this case, the effective diffusion coefficient is given by:

$$D_i^{t,eff} = \frac{\varphi}{\tau} D_i^t \qquad (4.12)$$

Figure 4.4. Illustration of Knudsen and molecular diffusion in random porous material [16].

CHAPTER 5: IONIC CONDUCTIVITY

Abstract

In Chapter 5, the basic theory of ionic conductivity is presented. The concept of conductivity is defined and the two types of point defects in the crystal lattice, Schottky and Frenkel are mentioned. Oxygen ion and proton conductivity are explained, with an emphasis on solid electrolytes.

5.1 Introduction

Ionic conduction is defined the movement of an ion from one site to another through defect in the crystal lattice of a solid or aqueous solution. The magnitude of the ionic conduction in solids is referred to as ionic conductivity and is measured in Siemens. It is calculated by:

$$\sigma = nZe\mu \qquad (5.1)$$

Where, n is the number of charge carriers per unit volume, Z is the atomic number, e is the elementary charge constant (therefore Ze is the charge) and μ is the ion mobility.

For the achievement of the movement of an ion through a crystal, a leap from an occupied site to a vacant one is necessary. The ionic conductivity can only occur if defects are present in the crystal. It is, therefore, perceived, that defects act as the charge carriers. Usually, ionic solids do not possess a large number of defects and the ion mobility is generally low in room temperature. An expression for the variation of ionic conductivity as a function of temperature is given by the Arrhenius equation:

$$\sigma = \frac{\sigma_O}{T} exp\left(\frac{-E_\alpha}{RT}\right) \qquad (5.2)$$

Where σ_o contains n and Ze as well as the attempt frequency and jump distance, E_α is the activation energy and T is the temperature.

The two simplest types of point defects are Schottky and Frenkel defects. Schottky defects are formed when oppositely charged ions leave their lattice positions, creating vacancies. These vacancies are formed in stoichiometric units, in order to maintain an

overall neutral charge in the ionic solid. The vacancies are then free to move as their own entities.

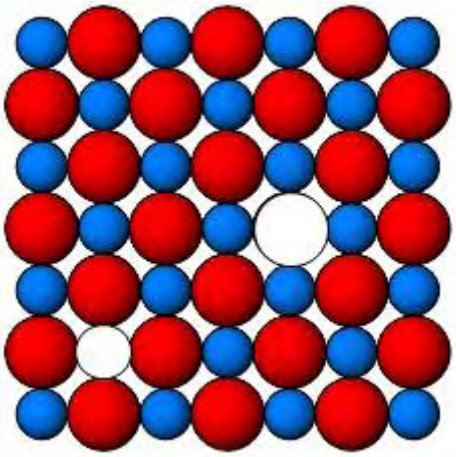

Schottky Defect
(i.e. NaCl)
$Na^+ + Cl^- \rightarrow V_{Na} + V_{Cl}$

Figure 5.1. Schematic representation of Schottky defects.

A Frenkel defect is formed when an atom or smaller ion (usually cation) leaves its site in the lattice, creating a vacancy, and becomes an interstitial by lodging in a nearby location, between other atoms or ions.

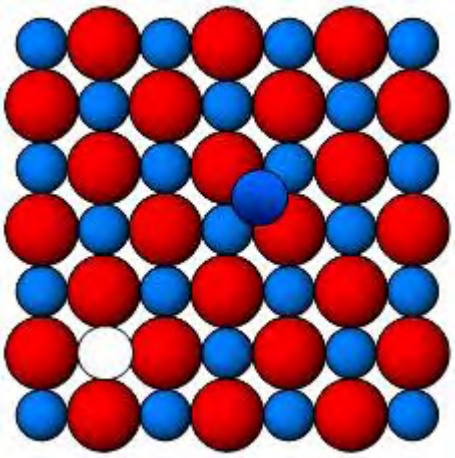

Frenkel Defect
(i.e. AgCl)
$Ag^+ \rightarrow V_{Ag^+} + Ag^+_{interstitial}$

Figure 5.2. Schematic representation of a Frenkel defect.

For solid electrolytes, the ionic conductivity ranges between 10^{-3}S/cm and 1S/cm. On the other hand, metals are characterized by electronic conductivity in a range between 10S/cm, and 10^5S/cm.

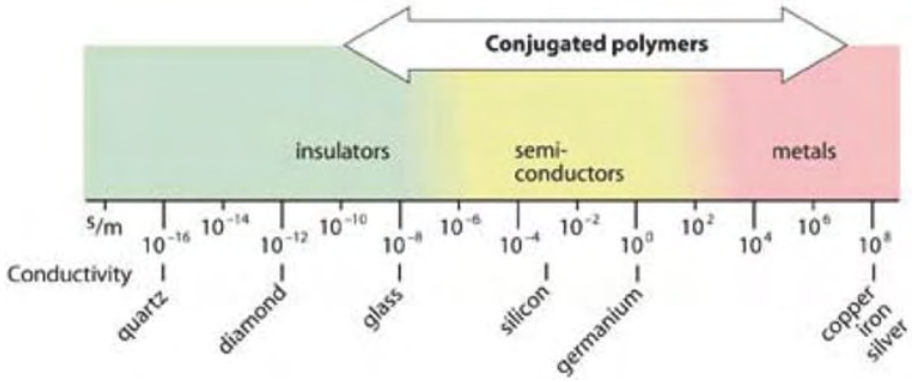

Figure 5.3. Classification of solid materials based on their conductivity.

There are two basic types of solid electrolytes in electrochemical devices, oxygen ion conductors and proton conductors.

5.2 Oxygen Ion Conductivity

Oxygen ion conductivity is defined as the movement of oxide ions through the crystal lattice (through oxygen vacancies). This movement causes the flow of current in oxygen ion conductors. This movement is a result of thermally-activated leaps of the oxygen ions, moving from one crystal lattice site to another.

Due to the strong temperature dependence of the ionic conductivity, solid electrolytes can display ionic conductivity values close to 1S/cm, which is comparable to the levels of ionic conductivity found in liquid electrolytes.

For oxygen ion conduction to occur, it is necessary that the crystal contains unoccupied sites equivalent to those occupied by the lattice oxygen ions.

5.3 Proton conductivity

Acting as electrolytes, high-temperature protonic conductors (HTPCs) must meet a wide range of requirements, including: high ionic (protonic) conductivity, excellent thermodynamic stability, high ceramic and mechanical qualities and acceptable thermal and chemical compatibility with other functional materials.

High-temperature protonic conductors are considered among the most promising electrolytes to be used in many applied fields, such as: solid oxide fuel cells (SOFCs), solid oxide electrolysis cells (SOECs), sensors, pumps and membrane reactors. The most known proton conducting materials are BaZrO3 (BZO) and BaCeO3 (BCO).

CHAPTER 6: ELECTROCHEMICAL DEVICES

Abstract

In the present chapter, some of the most important electrochemical devices are reviewed. At first, a brief historical review of fuel cells is cited, alongside with their operation, different types and application. Subsequently, the operation and utility of electrolyzers and supercapacitors are examined. Finally, the function and different types of electrochemical reactors are investigated.

6.1 Fuel Cells

The history of fuel cell goes back into the 19th century and is credited to Sir William Robert Grove. In 1839, he experimented on electrolysis, which is the decomposition of water into hydrogen and oxygen due to an electric current that passes through it. These experiments led to a device that was later called fuel cell. Grove thought that electrolysis could be reversed to produce electric energy from the reaction between oxygen and hydrogen. In order to examine that theory, he inserted two platinum electrodes into two separate sealed bottles, one containing hydrogen and the other oxygen. When these bottles were immersed in dilute sulfuric acid, electric current started flowing between the electrodes and water was formed in the bottles. Grove connected many of these devices in series, creating stacks, to increase the voltage produced.

A fuel cell is an electrochemical device which converts the chemical energy of a fuel directly into electrical energy. The basic compartments of a single cell are a porous anode and cathode separated by an electrolyte layer. The anode is the electrode where the oxidation of the fuel takes place, while in the cathode the oxidant, usually oxygen, is reduced. The electrodes are thin and porous sheets coated with the catalyst, which accelerates the electrochemical reactions. The electrodes are connected through an external circuit via which the electrons produced by the oxidation flow.

In a typical fuel cell design, hydrogen is supplied to the anode and the oxygen to the cathode. The electrochemical reactions take place at the electrodes to produce an electric current.

Anodic reaction: $H_2 \rightarrow 2H^+ + 2e^-$ (6.1)

Cathodic reaction: $2H^+ + \frac{1}{2}O_2 + 2e^- \rightarrow H_2O$ (6.2)

Overall reaction: $H_2 + \frac{1}{2}O_2 \rightarrow H_2O$ (6.3)

Protons (H^+) produced at the anode, flow through the electrolyte and react with oxygen and electrons at the cathode. Furthermore, the electrolyte prevents electrons from passing through it and creating a short circuit.

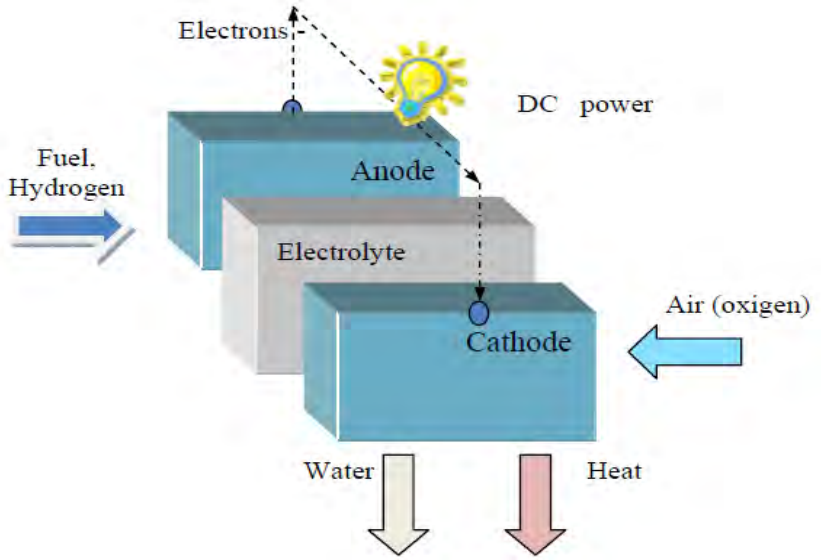

Figure 6.1. Typical concept of a single fuel cell [18].

There are many types of fuel cells available on the market, categorized by the type of electrolyte, the operative temperature range, the type of fuels which can be used, the type of catalyst used by the cell and the efficiency ratio of the energy conversion. Some of the most important types of fuel cells are:

- Polymeric Electrolyte Membrane Fuel Cells (PEMFC):
- Direct Methanol Fuel Cells (DMFC)
- Alkaline Fuel Cells (AFC)
- Phosphoric Acid Fuel Cell (PAFC)
- Molten Carbonate Fuel Cell (MCFC)
- Solid Oxide Fuel Cell (SOFC)

The higher efficiency of fuel cells is a consequence of the direct (chemical) production of electric energy from the fuel used. As a consequence, the technology is not affected by the limitations derived from the Carnot thermic cycle which burdens all the combustion based electric generation systems. The rate-determining step for the operation of a fuel cell is the reduction reaction. Therefore, efforts are made for the selection of the appropriate catalyst to accelerate this reaction. The more the reduction reaction is accelerated the higher the efficiency of the fuel cell.

Depending on the output power of the fuel cells, there are three basic fields of applications:

- Transportation (up to 70 kW)
- Stationary power applications (up to 500 kW)
- Portable power applications (up to some kW)

However, there are two main problems in developing the fuel cell applications: the need to provide a stable supply of pure hydrogen and to reduce the actual costs for the production of the cells. The first difficulty, regarding the supply of hydrogen, is the difficulty to achieve a highly efficient storage of hydrogen for long time periods. In addition to that, the cost for the production of hydrogen is high, increasing the cost of the fuel cell. Finally, Pt is the most effective catalyst for fuel cells. However, even if the Pt load in the electrodes is low, it raises the cost of the fuel cell.

Over the last decades, one of the basic goals of the scientific community is the decrease in the amount of Pt used and the increase of the utilization efficiency of the catalyst [18].

6.2 Electrolyzers

Hydrogen is the most common element in nature and can be used in a variety of chemical reactions, producing negligible pollutants since the only product of its combustion is water. It is of great importance, that the world market becomes independent of conventional energy sources and turn to renewable ones. Thus, hydrogen could be regarded as the fuel of the future.

However, hydrogen does not exist in its free form in nature but many chemical components consist of hydrogen atoms. For its extraction, energy is required. During the last years, several methods of hydrogen production have been developed and one of them is electrolysis of water.

Water electrolysis is a process in which hydrogen and oxygen are produced from water by applying an electric current. The simplest device for achieving this process is an electrolyzer, which consist of a number of electrolysis cells.

An electrolyzer is composed by an anode and a cathode and an electrolyte membrane between them. Both the anode and the cathode are in contact with gas channels and are also connected with a DC power source. Generally, both electrodes are supplied with steam through the gas channels. At the anode, water decomposition takes place producing hydrogen and oxygen ions:

$$H_2O + 2e^- \rightarrow H_2 + O^{2-} \quad (6.4)$$

At the cathode, decomposition of the water takes place according to the following electrochemical reaction:

$$H_2O \rightarrow \frac{1}{2}O_2 + 2H^+ + 2e^- \quad (6.5)$$

Protons are transferred through the electrolyte to the anode and form hydrogen:

$$2H^+ + 2e^- \rightarrow H_2 \qquad (6.6)$$

Hydrogen production in an electrolyzer is accomplished according to the above reactions (Eq. 6.4 – Eq. 6.6).

At the anode, oxygen ions that are formed in Eq. 6.4 move to the cathode where the form oxygen [19]:

$$O^{2-} \rightarrow \frac{1}{2}O_2 + 2e^- \qquad (6.7)$$

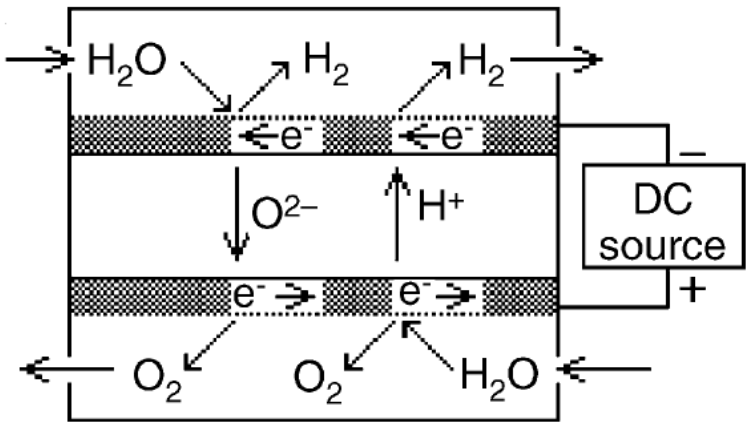

Figure 6.2. A schematic diagram of an electrolytic cell based on co-ionic electrolyte [19].

Many typed of electrolyzers have been studied and developed, based on the electrolyte and their operation temperature:

- Solid Oxide Electrolyzer (ceramic electrolyte, 850^{o}C)
- Polymer Electrolyzer (polymer electrolyte, 80^{o}C)
- Acid Electrolyzer (sulfuric or phosphoric acid electrolyte, 150^{o}C)
- Alkaline Electrolyzer (sodium or potassium hydroxide electrolyte, 80^{o}C)

The aforementioned electrolyzers use water as reactant to produce H_2 except for solid oxide electrolyzer which can also use CO_2 to produce CO [20].

Electrolyzers are considered as fuel suppliers for electrochemical devices (e.g. fuel cells) which use hydrogen to produce electric energy. They can also be used for the production of other fuels such as CO, which –by reacting with H_2 or by co-electrolysis of CO_2 and H_2O- can produce syngas. This product is combustible and is often utilized in internal combustion engines. In addition, electrolyzers are suitable for space applications, where hydrogen production and storage is of great value [21].

6.3 Supercapacitors

The forms of renewable energy used in generation plants are solar and wind energy. However, generation of such energy is not constant. In order for this problem to be solved, an energy storage system is essential thus the energy generation is continual [22].

As for energy storage and delivery, electrochemical capacitors are an efficient option. The storage process was discovered by Helmholtz in 1879. It was based on the separation of charged species in an electrolytic double layer [23]. It was Becker who created the first design of an electrochemical capacitor based on high surface area carbon, in 1957. However, capacitors were used more extensively in the 1990s, especially in hybrid electric vehicles [24].

Conventional capacitors are composed of two conducting electrodes separated by an insulating dielectric material. When a voltage is applied, opposite charges accumulate on the surface of each electrode. The dielectric keeps the charges segregated, producing an electric field; thus the capacitor stores energy. Capacitance C of the capacitor is defined as:

$$C = \frac{Q}{V} \qquad (6.8)$$

Where Q is the ratio of stored (positive) charge and V is the applied voltage. Capacitance is proportional to the surface area A of each electrode and inversely proportional to the distance D between the electrodes:

$$C = \varepsilon_0 \varepsilon_r \frac{A}{D} \qquad (6.9)$$

ε_o is the dielectric constant of free space and ε_r is the dielectric constant of the insulating material between the electrodes. The energy stored in a capacitor equals:

$$E = \frac{1}{2} CV^2 \qquad (6.10)$$

For the evaluation of power P, capacitors are generally represented as a circuit in series with an external load resistance R.

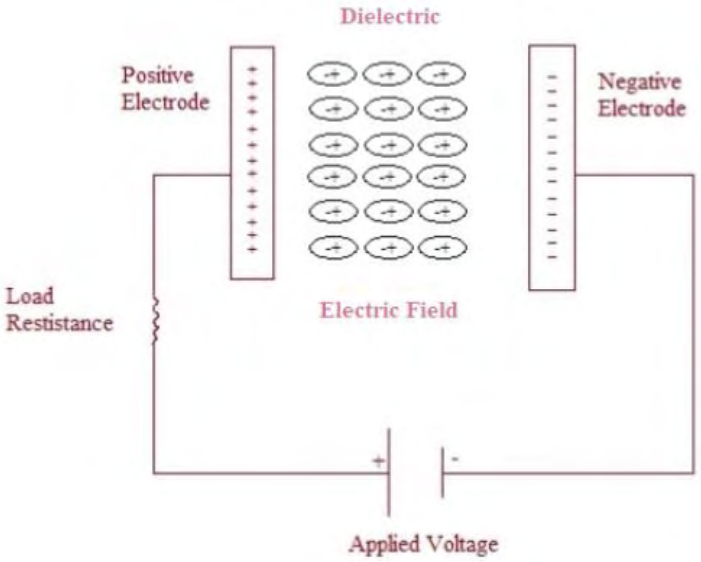

Figure 6.3. Representation of a capacitor as circuit in series with a load resistance.

The equivalent series resistance (ESR) includes, apart from the load resistance, the resistance originated by the internal components of the capacitor (current collectors, electrodes and dielectric material). The voltage during discharge is determined by these resistances. The maximum power P_{max} is:

$$P_{max} = \frac{V^2}{4ESR} \qquad (6.11)$$

Conventional capacitors have relatively high power densities, but relatively low energy densities when compared to electrochemical batteries and fuel cells. That is, capacitors store relatively less energy per unit mass or volume, but they are able to discharge it rapidly to produce high power values.

Electrochemical double-layer capacitors, also known as supercapacitors or ultracapacitors, display relatively high energy storage density simultaneously with a high power density [23]. They are dictated by the same principles are as conventional capacitors. However, their electrodes are characterized by much higher surface areas A and much thinner dielectrics that decrease the distance D between the electrodes, which leads to an increase in both capacitance C and energy E [25].

Typically, a supercapacitor is compiled by two electrodes, a separator and an electrolyte. The electrodes are constructed by a metallic collector, which is the high conducting part, and by an active material, which is the high surface area part. The separator is a membrane placed between the electrodes, allowing the mobility of charged ions and forbidding the electronic conductance. The assembly is impregnated with an electrolyte, which may be of solid state, organic or aqueous type. The working voltage of supercapacitor is determined by the decomposition voltage of the electrolyte and depends on the environmental temperature, the current intensity and the required lifetime [23].

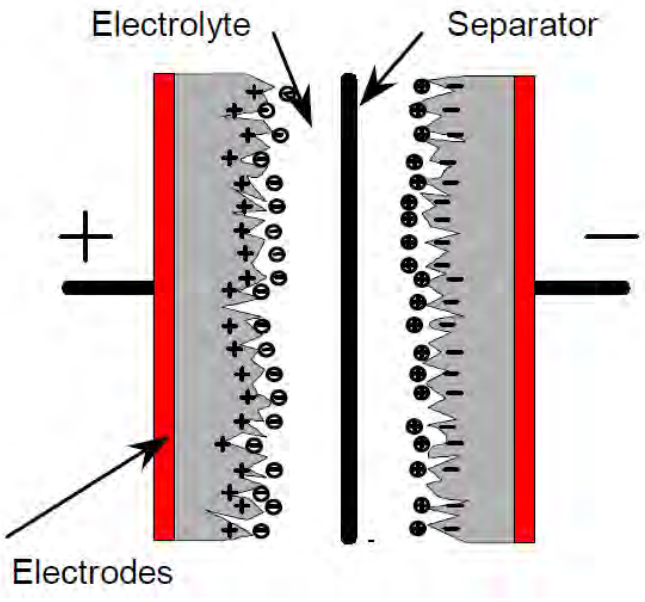

Figure 6.4. Sketch of a supercapacitor [23].

Among the advantages of supercapacitors are high power density, long lifecycle, high efficiency, wide range of operating temperatures, environmental friendliness and safety. These characteristics have made supercapacitors appropriate for applications in electric hybrid vehicles, digital communication devices such as mobile phones, digital cameras, electrical tools, pulse laser technique, uninterruptible power suppliers and storage of the energy produced by solar cells. On the other hand, their main disadvantages are high cost, high self-discharge rate and the fact that the values of energy density are not in desirable levels [26].

6.4 Electrochemical Reactors

Electrochemistry can offer major contributions to industrial processes, characterized by minimum waste production and low cost. Electrochemical engineering develops the practical knowledge and expertise of constructing and operating electrochemical reactors for the formation of chemical products such as inorganic compounds (e.g. Cl_2, concentrated NaOH and NH_3), organic chemicals and purified metals.

The design and operation principle of an electrochemical reactor is based on these of a typical electrochemical cell. The basic parts are an anode, a cathode and an electrolyte that separates them. The anode and cathode are fed with high values of direct current, and with the effect of the catalyst and the electrolyte, the electrochemical reactions take place. Usually, only one of the two reactions occurring in the reactor is of interest.

There is a variety of electrochemical reactor designs, depending on the requirements of the desirable process. The basic parameters are the shape, mode of operation and electrolyte flow, temperature control, number of electrodes, type of electrical connections and electrode structure. The decision for the cell selection is based on economic, engineering, technological, safety and environmental criteria [27].

There are two major reactor operation modes, based on the above characteristics:

- Batch operation, where the electrochemical cell is filled with the reactants and is operated during a certain time. The products are then separated from the solutions. Ideally, the entire volume is mixed without any concentration difference due to the stirring (stirred tank reactor). The conversion and most other conditions in the cell are changing with time [28].

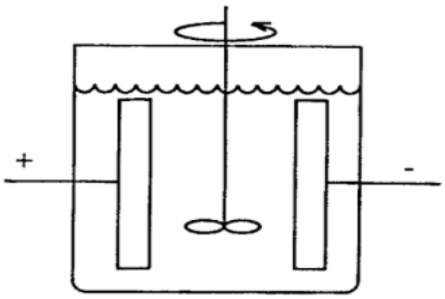

Figure 6.5. Schematic figure of single batch [27].

- Continuous operation (flow-through cell), where the cell is supplied with a continuous stream, which finally exits the cell after partial conversion. Steady state conditions are achieved after a certain period of time. Continuous operation is valuable for long-time stability tests of cell compounds such as electrodes and membranes. There are two limiting cases according to the mixing behavior within the flow:
    i. Backmix reactor with ideal mixing, which is similar to batch operation.

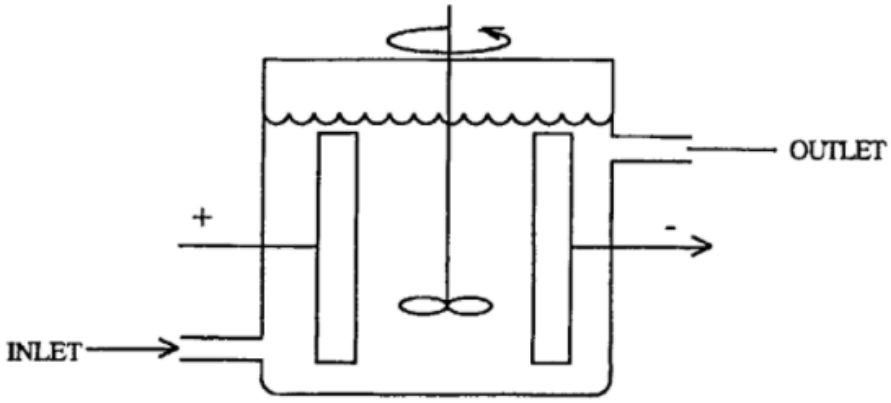

Figure 6.6. Schematic figure of continuous stirred tank (Backmix reactor) [27].

Plug flow reactor, where the flow moves through the cell along the electrode surfaces. Conversion and other operation conditions do not change with time (steady state), but they depend on the location between input and output of the cell [28].

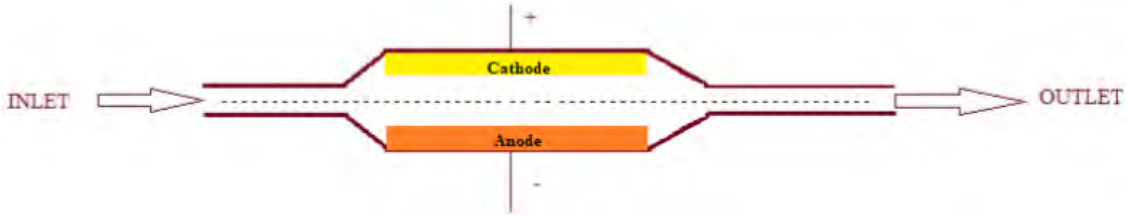

Figure 6.7. Schematic figure of plug flow reactor.

Although products are formed at both electrodes, the cell performance is determined with regard to the electrode where the desired product is formed. The current efficiency (CE) of an electrochemical reaction is the ratio of the electric charge used in generating the desirable product to the total charge Q passed through the reactor during a reaction. The current efficiency can be considered as the product yield based on the electrical charge:

$$CE = \frac{nF(Vol)}{Q}\Delta C_p \qquad (6.12)$$

Where Vol is the volume of reaction medium, n is the number of electrons, F is the Faraday constant and ΔC_p is the concentration change of the product over the course of the reaction.

The product selectivity (S_p) is the ratio of the moles of the product of interest to the total moles of products formed from the initial material:

$$S_p = \frac{number\ of\ moles\ of\ desired\ product}{\sum moles\ of\ all\ products} \tag{6.13}$$

The electrical energy required is given by:

$$Specific\ Energy\ Consumption = \frac{nFE_{cell}}{CE \cdot MW} \tag{6.14}$$

In the case of volumetric energy consumption, MW is replaced by V_m, which is the partial molar volume of the desired product. For constant current I over a time period t:

$$Specific\ Energy\ Consumption = \frac{E_{cell}It}{\Delta C_p (Vol) MW} \tag{6.15}$$

The space-time-yield (τ) is the mass of product per unit time that can be obtained in a certain electrochemical reactor of volume:

$$\tau = \frac{A_S \cdot I \cdot CE \cdot MW}{nF} \tag{6.16}$$

Where A_s is the active electrode area per unit reactor volume.

The aforementioned quantities characterize the performance and efficiency of an electrochemical reactor.

Electrochemical reactors offer significant advantages regarding the achievement of industrial and electrochemical processes. Some of the most important are versatility, energy efficiency, amenability to automation and cost effectiveness [29].

CHAPTER 7: ELECTROCHEMICAL SENSORS

Abstract

In Chapter 7, the electrochemical sensors are being reviewed. More specifically, a brief review of their history and future prospects is reported. The basic compartments and configuration are thoroughly examined. Finally, the operating principle of the electrochemical sensor is investigated.

7.1 History and Future Prospects

Throughout human history, people have lived and worked in dangerous environments, often exposed to toxic gases. Most of the times, the toxicity of the atmosphere was either poorly recognized or not recognized at all, leading to serious injuries or even deaths. Coal mines are major sources of combustible and toxic gases, while the oxygen level is low. Some of the first detection systems were open flame lamps. When the oxygen level was low, the flame would burn low as well. On the other hand, high levels of combustible gases would result in a growth of the flame's intensity. The problem with this detection system was that high concentrations of combustible gases would cause an explosion. An improvement on this method was the flame lamp, which contained the flame inside a glass barrel, while allowing the hot gases to escape through a flame-arresting wire mesh. Marks were also placed on the glass to allow a calculation of the presence of a combustible or the absence of oxygen.

In 1925, Dr. Jiro Tsuji used light-wave interference for the detection of combustible gases. In 1927, Dr. Oliver Johnson developed a method of detecting combustible gases using a platinum catalyst in a Wheatstone bridge electronic circuit [30]. If the platinum wire is maintained at a temperature of several hundred degrees then via catalysis it will detect any combustible gas which may be present in the atmosphere. The rise in temperature in the platinum wire leads to a resistance increase which may be measured. This is done via the resistance bridge circuit which typically provides an output signal.

In 1962, Seiyama et al. investigated thin film zinc oxide gas sensors based on the semiconductor catalysis mechanism. This was the first device which utilized the resistance change in a metallic oxide semiconductor which results from gas adsorption.

Taguchi introduced the stannic oxide ceramic gas sensor which led to the mass production of the world's first commercial devices. This production was further increased by the discovery of the sensitivity-improving properties of noble metal inclusions and the improvement of sintering procedures. Investigation on metal oxide sensors has been extended to other materials and the range of detectable gases has widened from combustible species to oxygen, oxides of nitrogen, hydrogen sulphide etc.

In the past, sensors were used for the detection of general combustible gases such as methane and carbon, but more recent studies focus on the development of sensors for specific purposes such as the detection of low concentration gases such as hydrogen sulphide, nitrogen oxides, mercaptans and general air pollutants [31].

Nowadays, the number of different gases that can be monitored by gas sensors has increased dramatically. Toxic or bad-smelling gases such as H_2S and NH_3 and hazardous gases such as AsH_3 and PH_3 are some of the main targets for contemporary gas sensors. The serious environmental crisis over the last years and the global issues of energy has also led to the development of sensors for the detection of air pollutants such as NO_x, SO_x and CO_2. Furthermore, gas sensors are applied for the control systems of combustion exhausts from stationary facilities and automobiles. In addition, the scientific community focuses developing biosensors technology in order to be applied to the human body [32].

7.2 Configuration

An electrochemical sensor is compiled by two or three electrodes in contact with an electrolyte. The electrodes are manufactured by placing a high surface area precious metal onto a porous hydrophobic membrane. The working (sensing) electrode is in contact with both the electrolyte and the gas of interest via the porous membrane.

i. The gas permeable membrane (hydrophobic membrane) covers the working electrode. It controls the amount of gas molecules reaching the electrode surface. It is usually made of thin, low-porosity Teflon. Such sensors are called membrane clad sensors. Alternatively, the membrane is made of high-porosity Teflon and the amount of gas molecules reaching the electrode is controlled by a capillary. Such sensors are referred to as capillary-type sensors. The membrane offers mechanical protection to the sensor and filters out unwanted particulates as well. The appropriate pore size of the membrane and capillary is important for the transfer of the desired amount of gas molecules. The pore size should be such as to allow a sufficient number of gas molecules to reach the sensing electrode and also prevent liquid electrolyte from leaking out or drying out the sensor.

ii. The selection of the electrode material is of great importance. It should be a catalyzed material which performs the electrochemical reaction over a long period of time. Noble metals, such as platinum or gold, are usually used for

an effective reaction with gas molecules. All three electrodes can be made of different materials to complete the cell reaction.

iii. The electrolyte facilitates the cell reaction and transfers the ionic charge across the electrodes. It should provide a stable reference potential with the reference electrode and show compatibility with materials used within the sensor.

iv. A scrubber filter can also be installed in front of the sensor to filter out unwanted gases. The most common is activated charcoal, which filters out most chemicals except for CO and hydrogen gases. The appropriate selection of the filter medium affects the sensor's selectivity to its target gases [33].

7.3 Operating principle

The operation of an electrochemical sensor is based on the reaction of the gas of interest, which generates electrical signal proportional to the gas concentration. It is compiled by a working (sensing), a counter electrode and a thin layer of electrolyte which separates them. The gas of interest passes through a small capillary, as it can be seen by Figure 7.1, and then is diffused through a hydrophobic membrane until it eventually reaches the sensing electrode's surface, where is either oxidized or reduced. The electrochemical reactions are catalyzed by the electrode materials, which are specifically selected for the gas of interest.

When the proper amount of gas reacts at the sensing electrode, a sufficient electrical signal is generated. The hydrophobic barrier also prevents the electrolyte from leaking out of the sensor. With the connection of a resistor across the electrodes, an external circuit is created and a current proportional to the gas concentration flows between the anode and the cathode.

The gas concentration is estimated by the measurement of the current. A stable and constant potential at the sensing electrode is essential for a sensor requiring an external driving voltage. This is accomplished by the introduction of a reference electrode within the electrolyte and in close proximity to the sensing electrode. A fixed stable constant potential is applied to the working electrode.

The reference electrode maintains the value of this fixed voltage at the sensing electrode. No current passes through the reference electrode. The current produced by the electrochemical reaction at the sensing electrode flows between the sensing and the counter electrode, is measured and is typically related to the gas concentration, according to Nernst equation. The value of the voltage applied to the sensing electrode makes the sensor specific to the analyzed gas [33].

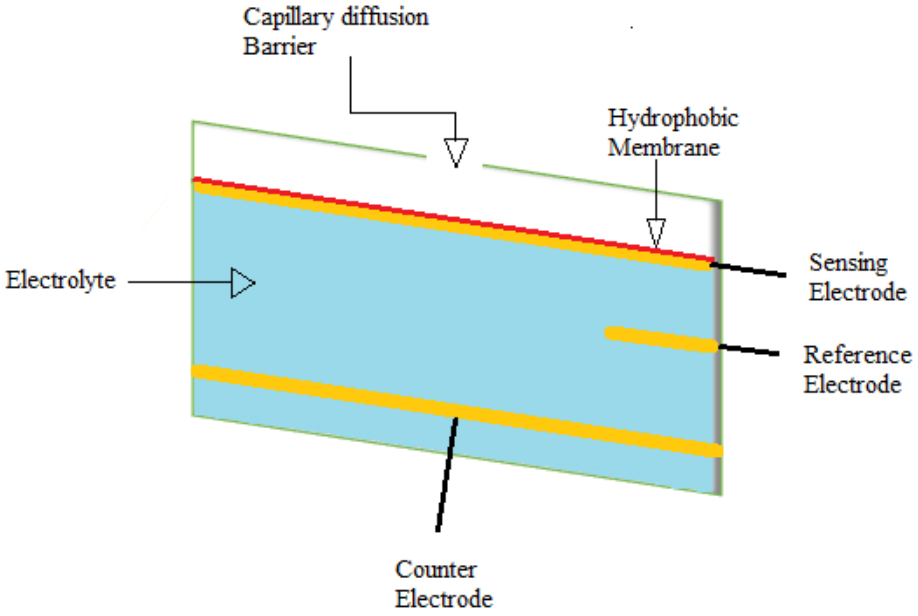

Figure 7.1. Typical electrochemical sensor setup.

A gas sensor is characterized by two basic functions. The first one is to recognize a particular gas species (receptor function) and the second one to transduce the gas recognition into a sensing signal (transducer function). The gas recognition is carried out through gas-solid interactions such as adsorption, chemical reactions and electrochemical reactions. The transducer function depends on the materials used for the gas detection. Gas recognition by semiconducting oxides is transduced into a sensing signal through the electrical resistance changes of the sensor elements, while capacitance can be used for the elements using dielectric materials. Other types of sensor material can use as sensing signals the electromotive force, resonant frequency, optical absorption or emission etc. Improving each function separately is the base for designing gas sensors. The promotion of the receptor function is important for increasing the enhancing the selectivity to particular species, while improving transducer function is important for augmenting the sensitivity [32].

The receptor system interacts with the analyte in selective chemical reactions and transforms the chemical information into a form of energy which may be measured by the transducer [34].

CHAPTER 8: CATEGORIES OF GAS SENSORS

Abstract

In the present chapter, the basic types and categories of electrochemical sensors are reported. The three categories of electrochemical sensors are i) solid electrolyte gas sensors, ii) resistive gas sensors and iii) impedancemetric gas sensors. At first, emphasis on solid electrolyte gas sensors and their further classification into potentiometric and amperometric is given. Subsequently, resistive and impedancemetric gas sensors are reviewed.

8.1 Solid electrolyte gas sensors

Especially solid-electrolyte sensors can successfully compete with other types of sensors and day by day they are finding wider practical applications [35]. They possess a number of advantages and often allow solving practical problems, which otherwise really cannot be solved. One of the advantages of such sensors is their stability. Among sensors, potentiometric and amperometric, solid-electrolyte sensors are most widely used [36]. Dependence of electrodes' potentials difference on concentration of the definite component in the analyzed gas is the basis for operation of potentiometric sensors. The sensing signal is an electromotive force (EMF) given by the Nernst equation. Potentiometric solid-electrolyte sensors for the gas composition control in various heat units [35-37] and measurements of oxygen in metal melts are widely used [38]. Non-equilibrium potentiometric sensors approach may be employed as an alternative one, when the gases at the interface between the electrode and the solid electrolyte are not in thermodynamic equilibrium [39-41]. Dependence of the limiting current on concentration of the defined component in the analyzed gas is the basis of the operation of an amperometric sensor. Solid state electrolyte gas sensors are further divided into potentiometric and amperometric sensors based on their operation.

8.1.1 Potentiometric gas sensors

The basic operation principle of potentiometric gas sensors are open-circuit conditions. Under these conditions, no ionic current flows through the electrolyte[42].

A potentiometric sensor consists of two electrodes separated by an electrolyte. The sensing electrode is immersed in the analyte and an equilibrium potential is established in the interface between the electrode and the electrolyte. The reference electrode, which is not in contact with the analyte, establishes a standard potential with regard to the electrolyte allowing the measurement of the potential of the sensing electrode by an external voltmeter. The voltage output of the potentiometric gas sensor is calculated by the Nernst equation, like any other electrochemical device:

$$E = E^{o} - \frac{RT}{nF}\ln(C) \qquad (8.1)$$

where C is the concentration of the analyte and for gases, C is the partial pressure of the gas [43].

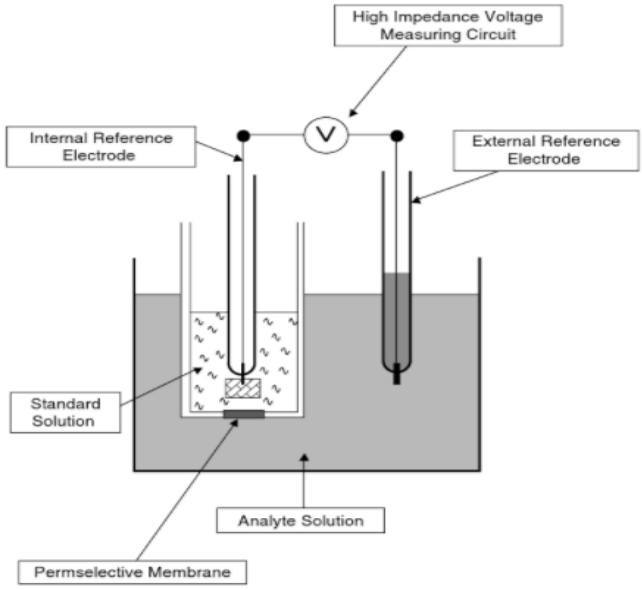

Figure 8.1 Simplest form of a potentiometric gas sensor [43].

Potentiometric gas sensors are used ideally for liquid solutions. For the measurement of various components in gas mixtures, such as O_2, NO_x, CO and other combustible components, amperometric gas sensors are used.

8.1.2 Amperometric gas sensors

The basic operation principle of the amperometric gas sensors is the linear variation of the limiting current of the electrochemical cell with the diffusion barrier of the analyzed component's partial pressure in the gas mixture [44].

The sensor is placed in the analyzed gas and its internal space is filled by the gas atmosphere. When voltage is applied between the sensor's electrodes, the gas

component's permeation from the internal to the external space is observed. In this way, the amount of the gas component pumped out from the sensor's interior is compensated with the amount permeating through the diffusion barrier. The gas component's flux is correlated with the sensor's electrical current, according to Faraday's law:

$$J(gas\ component) = \frac{I}{nF} \qquad (8.2)$$

where I is the current, n the number of electrons and F the Faraday's constant.

The flow of the gas component increases by increasing the voltage, until it reaches a certain value, when the concentration of analyzed gas inside the sensor becomes negligible. Then a limiting current (I_{lim}) is observed:

$$I_{lim} = \frac{2F \cdot D(gas\ component) \cdot S \cdot P}{RTL} \cdot p_{gas\ component} \qquad (8.3)$$

This equation can be used for low partial pressures, where, S is the capillary's inner diameter, P is the absolute pressure of the analyzed gas, R is the universal gas constant, T is the absolute temperature, L is the length of the capillary, $p_{(gas\ component)}$ is the partial pressure of the gas component and D(gas component) is the diffusion coefficient of the gas component, depending on temperature and pressure:

$$D(gas\ component) = D_o(gas\ component) \cdot \left(\frac{T}{T_o}\right)^m \frac{P_o}{P} \qquad (8.4)$$

Where D_o(gas component) is the diffusion coefficient at standard conditions (T_o,P_o) m is the coefficient which ranges from 1.5 to 1.9 for real gases [45].

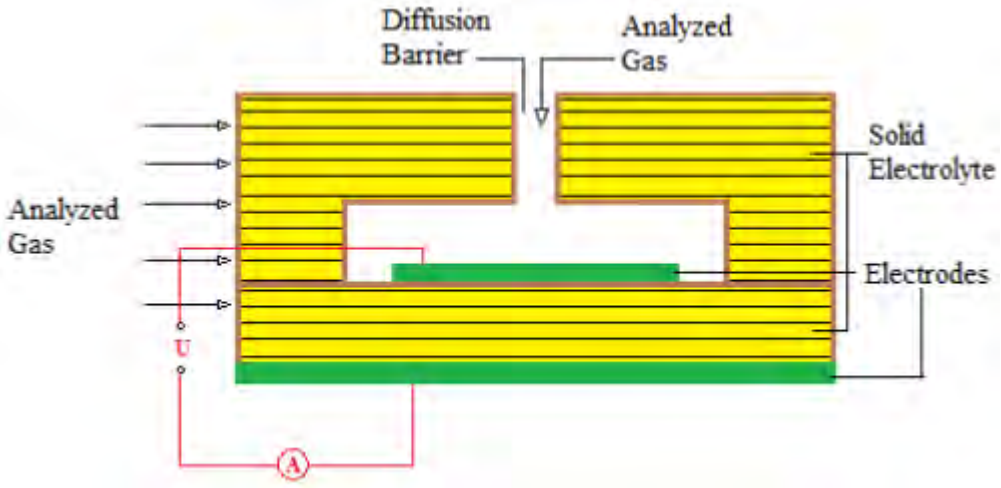

Figure 8.2. The working principle of amperometric sensor.

8.2 Resistive gas sensors

Another commonly used type of sensor is the resistive gas sensor. It is used for detecting hazardous or explosive gases in the air. This is due to the high sensitivity that characterizes the thin films (mostly tin oxide) towards reducing and oxidizing gases. Some of the many advantages of resistive gas sensors are simple configuration, easy fabrication and reasonable production cost.

The sensing electrode is a semiconducting metal oxide. It is supported by an inert substrate, which is connected to two metallic electrodes. Their operation is based on the measurement of electrical resistance changes between the semiconducting electrode and the analyte gas, when they come in contact. Ideally, the reaction between the sensor surface and the analyte gas is completely reversible. This procedure involves electron transfer.

Semiconducting resistive gas sensors can be divided into three categories: i) bulk conduction-based sensors, ii) surface conduction-based sensors and iii) metal/oxide junction-based sensors. Bulk conduction-based sensors are used as oxygen detectors at high temperatures (>500^{o}C). Surface conduction-based sensors, display satisfying sensitivity towards reducing gases such as CO, H_2 and HCs at low and medium temperatures. (200-500^{o}C). Metal/oxide junction-based sensors are used for monitoring O_2 at high temperatures operating like bulk conduction-based sensors. At low and medium temperatures they detecting exhaust gases such as CO, NO_x, SO_x and HCs working according to surface conduction mechanism [42], [46].

The main disadvantages of resistive gas sensors are low reproducibility and long-time stability due to aging. These drawbacks are enough to limit the field of applications of this type of sensors. Instabilities are caused by microstructural and morphological changes of the sensing elements and irreversible reactions with chemical species in the atmosphere. Furthermore, they are described by lack of selectivity. This happens because metal oxide-based gas sensors show cross-sensitivities, being sensitive to more than one species in the ambient [47].

8.3 Impedancemetric gas sensors

Impedancemetric sensors are the least developed of the above sensor types, showing, nevertheless, significant advantages. These advantages include capability to measure total NO_x concentration, high gas selectivity and precise detection on the single ppm level.

This type of sensor engages AC measurements at specified frequencies. This method is associated with solid-state impedance spectroscopy, a technique which measures cell response over a range of frequencies. This impedancemetric approach can be used by solid electrolyte-based or semiconductor-based sensors.

A sinusoidal voltage is applied at the solid electrolyte-based sensors and the occurring current is measured. The impedance is defined as the ratio of voltage to current in the frequency domain.

Impedance spectroscopy is applied for the detection of individual electrochemical components based on their frequency-dependent behavior. Sensors of this type are used for monitoring water vapor, HCs, NO_x and CO [42].

CHAPTER 9: HIGH TEMPERATURE ELECTROCHEMICAL SENSORS

Abstract

In this chapter, a detailed examination of electrochemical sensors with high operating temperature (up to 1000^{o}C) is being conducted. At first, the most important applications of such electrochemical sensors are reported. Furthermore, the properties of high-temperature proton-conducting materials, which are essential for the fabrication of high temperature sensors are presented. Subsequently, the most common types and applications of high temperature sensors, such as oxygen, combustible gas, nitrogen oxide and hydrogen sensors are thoroughly examined.

9.1 Introduction

One of the most crucial use of electrochemical gas sensors is the detection of exhaust gases produced during combustion processes, especially in automotive engines. The composition of exhaust gases for most engine types contains three basic pollutants: unburned or partially burned hydrocarbons (HCs), carbon monoxide (CO) and nitrogen oxides (NO_x), mostly as NO. For the optimization of a combustion process, information about the oxygen amount is necessary. The emission control is completed by monitoring the CO, HCs, and NO_x content. The exhaust gases, which can reach temperatures of up to 1000 ^{o}C, is essential to be detected directly right after the combustion. This is a challenge for many sensing technologies.

Sensing methods such as calorimetry, chromatography and spectroscopic techniques are too expensive and unwieldy for in situ measurements in a wide temperature range and chemically contaminated environments. The most reliable gas sensing technology for this type of environment is solid-state electrochemical sensors. Compared to other methods, they have high thermal stability, low cost, simple structure and fabrication, and compatibility with electronic systems. Over the last decades, a significant number of solid-state gas sensors have been investigated for high temperature processes (600-1000^{o}C) [42]. Recently, investigation is being conducted regarding the low and mid-temperature applications of electrochemical sensors. This type of sensors can be used in

combustion processes as well, in food industry, environment monitoring and medical diagnosis (biosensors).

9.2 Properties of high-temperature proton-conducting materials

The function of electrochemical sensors is based on a solid oxide proton-conducting material. Its selection should be such, so that it meets a set of properties such as ceramic, transport, thermomechanical characteristics as well as long-term stability and chemical stability.

The material selected as an electrolyte, should be characterized by proton-conductivity but negligibly low electronic and oxygen-ionic conductivity. The majority of oxide compounds showing proton transport are not pure proton conducting electrolytes. The response characteristics of potentiometric sensors are influenced by high electronic conductivity of a material, leading to a decrease of the electromotive force (EMF). For this type of sensors, high proton conductivity does not strongly affect the function of the sensor, because the ohmic resistance of the electrolyte does not affect the response of the sensor and the values of this characteristic.

Since the configuration of potentiometric sensors is composed of separated gas chambers, certain conditions are required: high relative density of the electrolyte, absence of porosity and tightness between the sensor components. The violation of any of these conditions is associated with the partial mixing of gases and results in a lower electrical potential difference value in comparison with the expected one.

In addition, all the sensor components must display fine stability in oxidizing, reducing atmospheres and corrosive environments at high temperatures. The measurements of the sensor must be reproduced for a long period of time.

Sensors based on proton-conducting electrolytes can operate at high temperatures, up to 1000^{o}C. Consequently, the functional materials should be thermally compatible, considering both the similar behavior of the materials expansion/shrinkage and close thermal expansion coefficients (TECs). The maintenance of sensor's integrity under operating condition is favored by the selection of thermally compatible materials. Specifically for potentiometric sensors, TEC affects the device's integrity and high porosity leads to the presence of gas-leakages. Furthermore, the sensors must possess high sensitivity to hydrogen and low cross sensitivity to other fuel gases (hydrocarbons, H_2S, CO), high stability of signal with low noise, appropriate reliability (signal uncertainty <10%), fast response and recovery time, indication of hydrogen in a required concentration range, small sensor size, simple orientation and maintenance with long service interval, simple system integration and interface, low power consumption under operation, and low cost [48].

9.3 Oxygen sensors

One of the most notable applications of solid-state gas sensors are oxygen sensors, which are used in automotive exhaust emission control systems. Particularly, the air/fuel (A/F) ratio, which is supplied into the engine, is monitored. That, in association with three-way catalysts, has reduced the gas pollutants emitted by automobiles. Moreover, a second oxygen sensor downstream is necessary for on-board diagnosis (OBD). This sensor monitors the O_2 storage capacity of the catalyst, which determines its working efficiency. The catalyst's efficient operation is indicated by oxygen storage while the reduction of NO_x occurs during the lean cycle and oxygen release during the oxidation of HCs in the rich cycle.

Potentiometric oxygen sensors are often used for the automotive exhaust emission control systems. For this type of oxygen sensor, usually air is employed as the reference gas electrode. The oxygen concentration can be estimated by the Nernst equation (9.1), where the open circuit potential (E^o) is given by:

$$E^o = (t_{O^{2-}}) \left(\frac{RT}{4F}\right) ln \left(\frac{P_{O_2}^{sensing}}{P_{O_2}^{reference}}\right) \qquad (9.1)$$

$P_{O_2}^{reference}$ and $P_{O_2}^{sensing}$ are the oxygen partial pressure at the reference and the sensing electrode respectively, and $t_{O^{2-}}$ is the transport number for oxide ions, which equals one for a solid electrolyte [42].

The most common solid electrolyte for high temperature gas sensor is yttrium partially stabilized zirconia (YSZ) or its derivatives. YSZ is structurally and chemically stable up to 1600°C. The main disadvantage of YSZ-based oxygen is the use of external Pt/air as the reference gas electrode, because it prevents the miniaturization of the sensors. With the external air reference, the sensor can only measure the oxygen concentration near the wall of the combustion chamber. By removing this reference electrode, then oxygen sensors of smaller size and simpler configuration can be manufactured and placed inside the combustion environment. This way, more precise measurements are acquired. Instead of external air reference electrode, an internal metal/metal oxide electrode can be used. The internal electrode can provide a stable equilibrium oxygen partial pressure for the gas mixture at a specific temperature. Among the metal/metal oxide systems investigated, such as In/In_2O_3, Sn/SnO_2, Pd/PdO, Ru/RuO_2 and Ni/NiO, only the latter can work properly under high temperatures.

The Ni/NiO-based oxygen sensor was investigated by Chowdhury *et al.* and found to have an accurate and fast response with good recovery characteristics in a temperature range of 600-1400°C. In order to prevent alloy formation among Ni and Pt, an Al_2O_3 isolation layer was also employed in the design of the sensor. Hence, improvement in the performance and stability of the sensor was accomplished. Nevertheless, extensive use of the sensor over a long period of time demeaned its performance. This was caused by grain growth and sintering of the internal electrode at high temperatures.

Rajabbeigi *et al.* studied solid CeO_2 (with 25mol% ZrO_2) and CeO_2-ZrO_2-TiO_2 as reference electrodes, which at high temperatures store oxygen and acts as the reference oxygen source as well. Although these sensors responded to oxygen concentration changes, they exhibited a limited voltage (EMF) range around the stoichiometric A/F ratio, in comparison with the external Pt/air reference electrode.

More investigation and research efforts are required to develop air reference free oxygen sensors at high temperatures of up to 1000ºC.

Although the stoichiometric point in the combustion process can be measured with a potentiometric oxygen sensor, potentiometric measurements are difficult in lean combustion gas with a high concentration of oxygen. Thus, for the detection of a wide range of oxygen concentrations, a limiting-current measurement that depends linearly on oxygen concentration is desirable. The limiting current is given by:

$$I_{lim} = \frac{4FD_{O_2}P_{tot}A}{RTL}\ln(1 - x_{O_2}) \quad (9.2)$$

Where L and A are the length and the cross section of the diffusion channel respectively, $D_{O_2}$is the oxygen diffusion coefficient, Ptot is the total gas pressure and $x_{O_2}$is the molar fraction of oxygen in the gas.

For oxygen concentrations below 10%, the limiting current is approximately estimated by:

$$I_{lim} = -\frac{4FA}{RTL}D_{O_2}P_{O_2} \quad (9.3)$$

Amperometric oxygen sensors can accurately accomplish measurements with high sensitivity (ppm to ppb). On the other hand, they display poor thermal and long-term stability alongside with the difficulty in designing the diffusion barrier.

Apart from YSZ, Gd or Sm doped CeO_2 materials have been studied and found to be suitable as solid electrolytes for high temperature applications. One of the materials that exhibited promising results, is $Ce_{0.8}Sm_{0.2}O_{1.9}$. In comparison with YSZ, it has shown higher ionic conductivity and can be used as a solid electrolyte for amperometric oxygen sensors at 500-700ºC. Regarding the materials of the diffusion barrier, certain conditions such as high electronic conductivity and good thermal stability need to be fulfilled. Cobalt containing perovskites, such as LCO, have exhibited good diffusion control, high electronic and oxygen ion conductivity and high electrochemical catalytic activity as well.

Due to limited literature reports of high temperature oxygen gas sensors, innovative devices combining several cells are being developed. Some cells can work in amperometric mode as oxygen pumps, while the rest in potentiometric mode as oxygen gauges. With this design, the accuracy of measurements is increased [42].

Another type of oxygen sensor appropriate for high temperature applications is the resistor-type oxygen sensor. This type of sensor is based on the bulk conduction mechanism at temperatures above 800 ºC. The conductivity of semiconducting metal oxides changes along with with the concentration of charge carriers (electrons for n-type

and holes for p-type semiconductors). The bulk defect species have high mobility at the temperature range of 700-1100 ^{o}C. Therefore, the non-stoichiometric oxide reaches equilibrium by reacting with the gas species in the surrounding environment, alterating the charge carrier concentration. Thus, the bulk conductivity of the metal oxide is determined by the ambient gas species composition, which defines the concentration of the analyte gas.

For the oxygen sensing mechanism of n-type semiconductors, oxygen vacancies ($V_O^{\cdot\cdot}$) in the bulk oxide react with the oxygen molecules (O_2), incorporating two electrons to form a lattice oxygen ($O_O^{\times}$). Depending on the oxygen partial pressure, the reverse reaction can also take place:

$$O_O^{\times} \leftrightarrow V_O^{\cdot\cdot} + 2e^{-} + \frac{1}{2}O_2 \qquad (9.4)$$

According to the reaction above, when the oxygen partial pressure is increased, the concentration of electrons in n-type metal oxides is decreased, leading to a decrease in the bulk conductivity. The electrical conductivity is given by:

$$\sigma = Aexp\left(-\frac{E_A}{KT}\right)P_{O_2}^{\frac{1}{m}} \qquad (9.5)$$

Where E_A is the activation energy and P_{O_2} is the oxygen partial pressure. The absolute value of m depends on the dominant defects involved in the reaction between oxygen gas and the sensing material, typically varying between 4 and 6. The lower the value of m, the greater sensitivity to changes in the oxygen partial pressure the sensor exhibits. Consequently, the semiconducting metal oxide which is used should have small m and E_A values to obtain high oxygen sensitivity and low interference from temperature fluctuations.

Over the last years, some of the metal oxides which have been thoroughly investigated as resistive oxygen sensing materials are titanium dioxide (TiO_2), niobium pentoxide (Nb_2O_5), gallium oxide (Ga_2O_3), cerium oxide (CeO_2) and perovskite strontium titanate ($SrTiO_3$). Although all of these materials display promising results regarding resistor-type oxygen sensors at high temperature, the high temperature dependency of their conductivity hinders their practical application. Two approaches have been proposed to design temperature independent resistive oxygen sensors. The first one is the use of a supplementary temperature compensating material. It must be insensitive to the oxygen partial pressure and exhibit similar temperature dependence to the oxygen partial pressure measurement materials. The second one is the use of a material, which has an intrinsic temperature independent conductivity.

More investigation and experiment efforts are required to further improve the reliability and long-term stability of resistive oxygen sensors for high temperature applications [42].

9.4 Combustible gas (CO and HCs) sensors

In order to monitor more gas pollutants in combustion processes, CO and HCs sensors are used. The fact that the concentrations to be detected are as low as a few ppm and the operating temperatures are between 800-1000 ^{o}C, makes the development of such sensors more difficult. In situ monitoring of CO can evaluate the fuel combustion efficiency, since CO is produced when the carbon of the fuel is not fully burned, and can provide feedback to control systems as well. On the other hand, in rich combustion conditions, unburned hydrocarbons may appear. High temperature HCs sensors are employed downstream of a three-way catalytic converter (TWC), to measure the limited components directly. This provides on-board diagnosis and more precise results than dual oxygen sensors.

There are two operation modes for CO and HCs sensors, resistor-type and mixed potential-type. Both of them usually work under low or mid temperatures (up to 600 ^{o}C).

It is extremely difficult for resistor-type sensors to detect CO and HCs with good recoverability, reproducibility and stability at high temperatures. This is due to the fact that CO and HCs react with lattice oxygens in oxides to form oxygen vacancies. Consequently, there are very few metal oxides which can be used to detect reducing gases (CO and HCs) in high temperatures. Fleischer *et al.* studied pure Ga_2O_3 and SnO_2 doped Ga_2O_3 in the temperature range of 600-1000 ^{o}C. They exhibited stable, sensitive and recoverable responses towards both CO and HCs, but suffered from high cross sensitivity. Adding a gold dispersion, can lead to an improved Ga_2O_3 sensitivity to CO. It was also found that increasing the operating temperature the sensitivity of the resistor-type sensors decreases. Hence, the sensitivity of the sensor at high temperature is important to evaluate its efficiency. Apart from that, the selectivity of the sensor at high temperature is the most challenging factor, due to the nature of the sensing mechanism.

Most of the CO and HCs sensors use the mixed potential principle. The EMF between two different electrodes provides the sensor signal. One electrode is usually made of a catalytically active conductor such as platinum. The other electrode (counter) is made of a catalytically inactive material such as gold. YSZ is the most common solid electrolyte and there are also a few studies on β-alumina and $Ce_{0.8}Ga_{0.2}O_{1.9}$. Some oxides such as WO_3, Nb_2O_5 and Nb_2O_5-Ta_2O_5 were found to work properly as sensing electrodes at 500-700 ^{o}C, by Di Bartolomeo's research group. Apart from simple oxides, doped-oxides and perovskites have also been studied. Brosha *et al.* experiment with $LaCoO_3$ and $La_{0.8}Sr_{0.2}CoO_{3-\delta}$ as sensing electrodes, YSZ as the electrolyte and $LaMnO_3$ as the counter electrode for CO and HC detection at 700 ^{o}C. This configuration displayed good stability. Due to reaction mechanisms that occur in mixed potential sensors, most of them have poor selectivity. Furthermore, they have also high cross sensitivity, because both CO and HCs are oxidized to produce electrons for the reduction of the oxygen [42].

9.5 Nitrogen oxide sensors

Detecting NO_x in various areal spaces is important for health and environment. NO_x is one of the main causes of acid rain and in urban areas concentrations can go up to dangerous levels for health, especially around the sites of heavy traffic. Specifically, exposition to NO_2 can cause serious effects to human nerve and respiratory system [49]. In combustion exhaust 7-80% of the total NO_x content is NO, because of its stability at high temperatures (>500^{o}C). Therefore, the detection of NO and NO_2 emission are of crucial importance.

Generally, NO_x sensors should meet certain conditions such as: i) endurance at high temperatures (600-900^{o}C) for long periods of time and ii) insensitivity to moisture and ability to provide a stable signal, even in the absence of oxygen. NO_x sensors are divided, according to their operation mode, into amperometric, mixed potential and impedancemetric NO_x sensors.

The most successful and commercially available type of NO_x sensor is the amperometric. It is compiled by two chambers; the first one works as an oxygen pump to extract the oxygen that comes from the automobile exhaust. In the second chamber, decomposition of NO into N_2 and O_2 occurs and the O_2 level is monitored by an amperometric zirconia-based sensor. Amperometric NO_x sensors exhibit high durability and accuracy in the measurements, with only moderate degradation in signal after long periods of time. Nevertheless, their high cost and complex design are an obstacle for their extensive use. This is why efforts and investigations for the proper electrode and electrolyte materials are being conducted. The ability of maintaining good response and selectivity above 700^{o}C, are significant for high temperature automotive applications of NO_x sensors. Recent experiments have led to the design and development of an amperometric sensor using YSZ as an electrolyte and nano-structured perovskite-type oxide $Gd_{0.2}Sr_{0.8}FeO_{3-\delta}$ impregnated on porous YSZ as a sensing electrode.

Resistor-type sensors based on WO_3 have been used as well for the measurement of NO_x at high temperatures, but have not displayed the desired selectivity and stability. As for potentiometric NO_x sensors, the suitable materials do not have the required properties under high temperatures. Mixed potential sensors have been developed to eliminate these drawbacks by using galvanic cells composed of electrode materials with different catalytic activities.

Mixed potential NO_x sensors should have a sensing material with excellent thermal stability to meet the requirements for high temperature sensing. NiO and other Ni oxides are found to be the most suitable materials for high temperature sensing electrodes (>800^{o}C). The sensors that possess NiO sensing electrodes have given satisfying results in NO_2 detection. These electrodes have showed good sensitivity in wet and dry atmospheres. NiO is the oxide which gives the highest NO_2 sensitivity and also operates at the highest sensing temperature. The addition of a noble metal (Pt, Rh, Ir, Pd and Ru) have led to enhancement in the sensing properties of NiO-based NO_x sensors. Rh gives the most significant improvement in NO_2 sensitivity.

One of the biggest difficulties for NO_x sensors is the detection of the total amount of NO_x ($NO+NO_2$). The opposite dependence of the sensor on NO and NO_2 can result in response compensation in the real exhaust emitted by vehicles. This could be solved by converting NOx into NO_2 before the measurement takes place by using an oxidation catalyst electrode.

Impedancemetric NO_x sensors are the least developed type. They have shown prospect in monitoring NO_x at lower ppm levels. Compared to mixed potential NO_x sensors, the responses of impedancemetric sensors to NO and NO_2 are of the same sign and similar magnitude; this indicates that they can measure the total amount of NO_x. Miura *et al.* reported an impedancemetric YSZ-based NO_x sensor with a $ZnCr_2O_4$ sensing electrode. The sensor showed almost the same sensitivity towards NO and NO_2 at 700 ^oC.

The above sensor is an example of the many that have been investigated. To this point, studies and experiments focus on eliminating the interference from O_2 concentration variations in the gas sample, which incommodes the sensing performance of the sensor. Furthermore, impedancemetric sensors require more complicated signal processing equipment and electronics [42].

9.6 Hydrogen sensors

Recently, solid electrolytes with proton conductivity have attracted increasing attention of researchers. These materials can be applied to electrochemical devices that operate under medium and high temperatures, such as hydrogen sensors.

A number of studies have focused on the development of potentiometric sensors for the detection of hydrogen. The biggest challenge in creating potentiometric hydrogen sensors is the selection of the reference electrode, which should provide a constant potential at the operating temperature of the sensor (>600 ^oC). For these reasons, a large number of investigations are devoted to the development of proton conducting solid electrolyte materials [44]. Specifically, high-temperature proton-conducting (HTPC) ceramic materials have been studied because of their potential applications, including hydrogen sensors, fuel cells, electrolysis cells, reactors for hydrogen production and ammonia synthesis as well. The wide range of applications is linked to the appearance of proton transport properties in solid oxides under hydrogen-containing environments.

The sensors based on HTPC ceramic electrolytes can be used effectively in combustion processes control systems, monitoring various chemical pollutants and determining the concentration of hydrogen-containing compounds in the exhaust gases.

Most studies focus on hydrogen sensors based on the potentiometric mode of operation. Amperometric, resistive and impedancemetric gas sensors are also investigated but attracted less attention.

Iwahara et al. designed a hydrogen sensor based on proton-conducting ceramic materials for the first time. They used a material with $BaCe_{0.9}Nd_{0.1}O_{3-\delta}$ (BCN) composition in a concentration cell of H_2,Pt|SCY|Pt,H_2+Ar type, which imitated the

operation of the hydrogen sensor. The BCN material was selected because it displays higher conductivity than SCY and its conductivity can be considered as predominantly ionic in wet reducing atmospheres. Good accuracy of the sensor and high-speed response show the effectiveness of such sensor design.

Kalyakin *et al.* fabricated a hydrogen sensor based on two electrochemical Pt|BCZY|Pt cells, where BCZY is $BaCe_{0.7}Zr_{0.1}Y_{0.2}O_{3-\delta}$. This sensor is able of operating in both potentiometric and amperometric mode. Its operation is based on the presence of a diffusion barrier in the cell and the different polarity of the voltage applied to one of the electrochemical cells. In the case of potentiometric mode, hydrogen permeates through the electrolyte from the analyzed gas to the interior of the sensor. This way, the internal space of the sensor has an atmosphere close to pure H_2. The second electrochemical cell provides the electrical potential difference value (E). Thus, according to the Nernst equation:

$$E_H = \frac{RT}{2F} ln\left(\frac{p'H_2}{p''H_2}\right) \qquad (9.5)$$

the partial pressure of hydrogen in the analyzed gas ($p''H_2$) in relation to the reference atmosphere ($p'H_2 \approx$ 1atm). When the polarity of the applied voltage (U) is changed, the inverse hydrogen-ion flow initiates through the electrolyte, resulting in hydrogen depletion in the atmosphere inside the sensor under high values of U. Considering the current level (I), it can be found that this parameter increases at first and then does not change with further increase of U. This condition corresponds to the limiting current (I_{lim}), which is a linear function of $p''H_2$ [48].

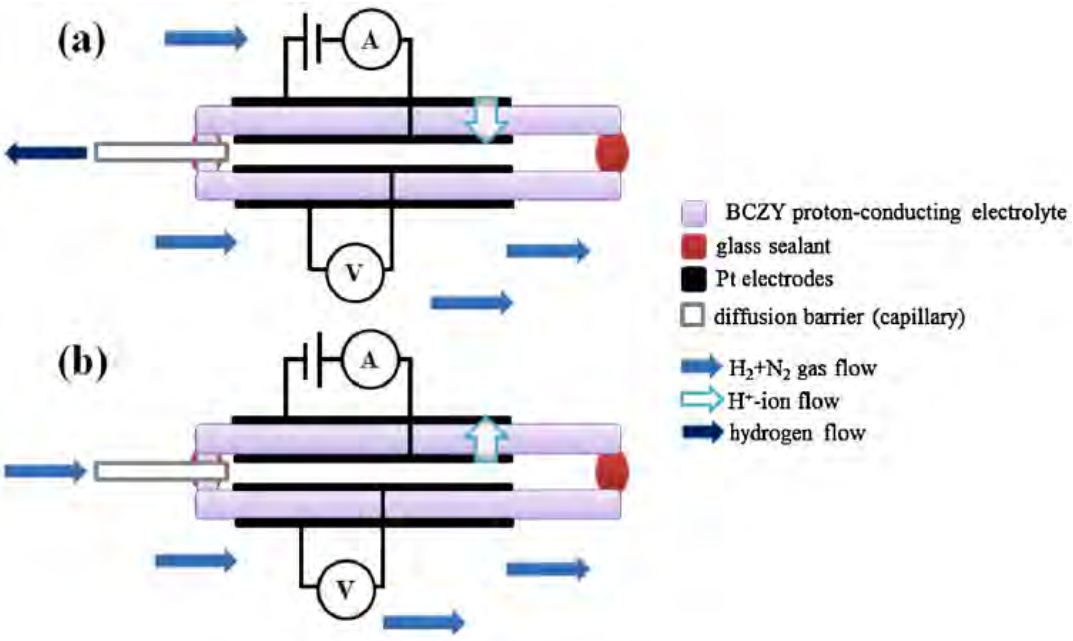

Figure 9.1. The scheme and working principle of the sensor in potentiometric (a) and amperometric (b) modes [48].

Regarding the amperometric operation mode, perovskites have the highest conductivity among the high temperature proton-conducting solid electrolytes; especially those based on barium cerate ($BaCeO_3$) and strontium cerate ($SrCeO_3$). However, due to their low chemical stability in CO_2-containing atmospheres, more perovskite materials, such as $LaYO_3$, $CaTiO_3$ and $CaZrO_3$ have been investigated. Tsiakaras *et al.* have recently reported $La_{0.95}Sr_{0.05}YO_3$, $CaTi_{0.95}Sc_{0.05}O_3$ and $CaZr_{0.9}Sc_{0.1}O_3$ as proton conducting solid electrolytes for high temperature hydrogen sensors, at operating temperature of 800^{o}C.

In the studied sensors, both the porous solid electrolyte and the leakage between the two linked solid electrolyte discs can be a diffusion barrier. The atmosphere inside the chamber is different at different stages of the cell operation. At the first stage, a nitrogen-hydrogen-steam mixture is contained in the interior of the sensor. At the inner platinum electrode, the reaction that takes place is:

$$H_2 \rightarrow 2H^+ + 2e^- \qquad (9.6)$$

As the cell voltage increases, the hydrogen content within the cell decreases because of the higher rate of hydrogen pumping out. At the second stage, when the gas mixture inside the cell is depleted with oxygen, the cell resistance sharply increases, as well as the current and the voltage. This current is the limiting current. The slight increase of the current from this point on, can be connected with the presence of electronic conductivity in the electrolytes, which is considerably lower than the ionic conductivity. The lower limit of the electronic transport number can be estimated as the ratio of the slope of the plateau to the slope of the V-I curve at V=0. In the third stage, the reaction that occurs at the inner electrode is:

$$H_2O \rightarrow 2H^+ + 0.5O_2 + 2e^- \qquad (9.7)$$

Hence, oxygen appears inside the cell and a mixture of nitrogen-steam-oxygen is formed in the interior of the sensor. The current at the third stage could be attributed to the ion transport. It was concluded that a sensor based on $La_{0.95}Sr_{0.05}YO_3$ with the porous diffusion barrier can be suitable for the monitoring of gas mixtures with medium and high (up to 100%) hydrogen content. In addition, a sensor based on $CaZr_{0.9}Sc_{0.1}O_3$ is appropriate for the monitoring of gas mixtures with low hydrogen content.

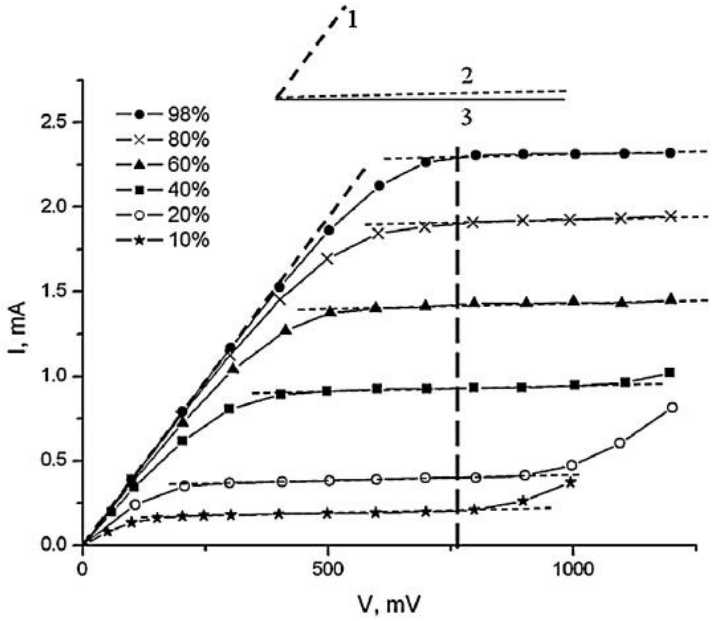

Figure 9.2. Voltage-current curves of $La_{0.95}Sr_{0.05}YO_3$ –based sensor on hydrogen content at different high hydrogen content in theN_2+ 2% H_2O + H_2 mixture, T = 800◦C. Line 1 gives the slope of the V-I curves tangent at zero point. Line 2 gives the "plateau" slope. Line 3 is the horizontal one [44].

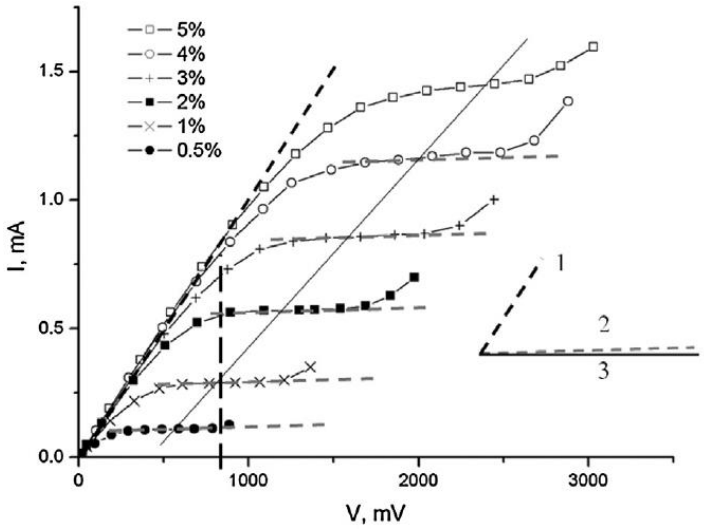

Figure 9.3. Voltage-current curves of $CaZr_{0.9}Sc_{0.1}O_3$ –based sensor at different low hydrogen content in theN_2+ 2% H_2O + H_2 gas mixture, T = 800◦C. Line 1 gives the slope of the tangent to V-I curves at zero point. Line 2 gives the "plateau" slope. Line 3 is the horizontal one [44].

CHAPTER 10: INTERMEDIATE TEMPERATURE ELECTROCHEMICAL SENSORS

Abstract

In the present chapter, a more detailed review on electrochemical sensors with intermediate operating temperature is conducted. More specifically, hydrogen sensors – amperometric and combined amperometric and potentiometric- are reported. Afterwards, hydrogen, carbon monoxide and methane sensors, as well as oxygen and humidity electrochemical sensors are reviewed.

10.1 Hydrogen sensors

10.1.1 Amperometric sensor

$LaYO_3$ was studied at first by Iwahara and Takahashi and it was observed that it displays proton conductivity. Recently, the scientific community has turned again into the investigation of $LaYO_3$ for possible mid and low-temperature applications. Tsiakaras *et al.* composed a Sr-doped $LaYO_3$ to examine the performance of the proton conducting electrolyte at intermediate temperatures. After the synthesis of the material, it was transformed in highly dense ceramic samples to examine the thermal and electrical properties. Then, a hydrogen sensor cell, made by the as prepared Sr-doped $LaYO_3$ dense ceramic samples, was used for the electrochemical characterization and hydrogen content measurements in $N_2 + H_2$ mixtures.

As it can be seen by Figure 10.1 the sensor is compiled by two electrolytes, which are shaped in the form of discs with cut segments. The first one is oxygen-ionic YSZ and the second is proton-conducting $La_{0.9}Sr_{0.1}YO_{3-\delta}$. Each disc has the recess on the one side. Platinum electrodes were coated and sintered at 1150^{o}C for 1 hour, on each electrolyte's opposite side. Thus, good adhesion between the electrodes and the electrolytes is achieved. The ceramic capillary (20mm length and 0.26mm inner diameter) was placed between the discs, which are pressed together and glued by high temperature sealant. Afterwards, the sensor was inserted in the oven, through which the N_2 and H_2 mixture (purity 99.9%) passed.

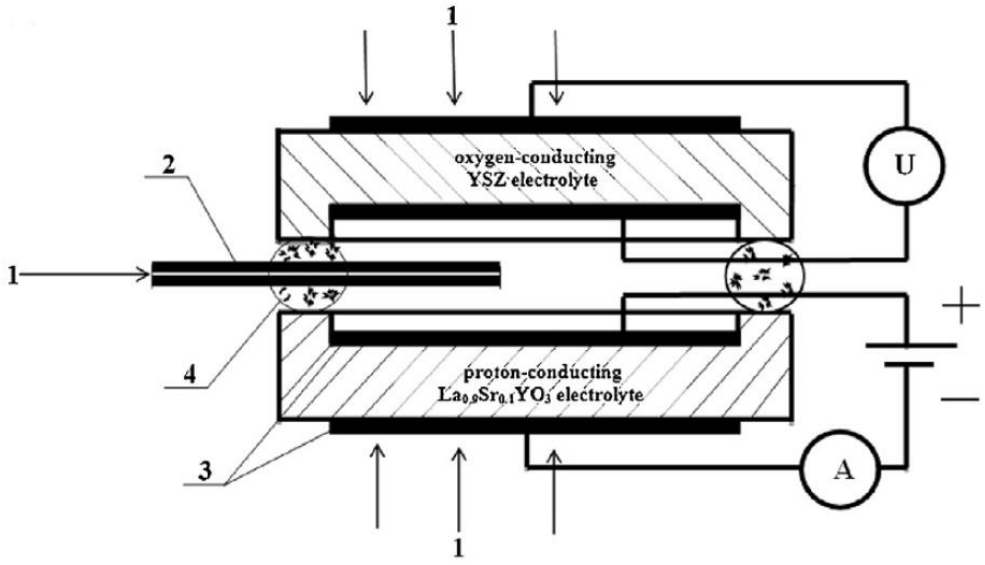

Figure 10.1. The principal scheme of the examined sensor. 1—the analyzed gas, 2—the diffusion barrier (capillary), 3—the electrodes and 4—the glass sealants.

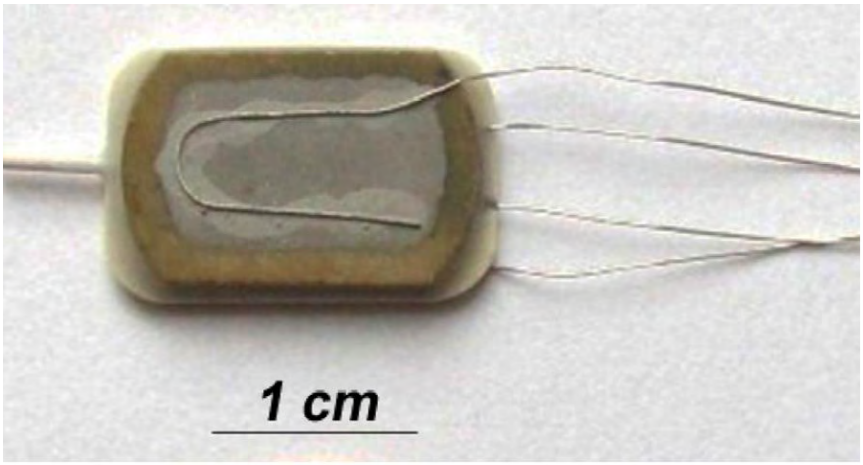

Figure 10.2. The experimental cell of the examined sensor.

Voltage is applied between the electrodes of the $La_{0.9}Sr_{0.1}YO_{3-\delta}$ electrolyte. Thus hydrogen is pumped out from the interior of the cell and a current is measured. At the YSZ cell the changes in oxygen partial pressure are measured in the internal side of the sensor, while hydrogen is being pumped out. The oxygen partial pressure can be found by:

$$pO_2 = \left(\frac{K \cdot pH_2O}{pH_2}\right)^2 \qquad (10.1)$$

The hydrogen partial pressure decreases while hydrogen is pumping out from the interior of the sensor. The change that is measured is the difference between the hydrogen partial pressure in the open circuit, and the pressure during hydrogen pumping out:

$$\Delta V_{OC} = \frac{RT}{4F} ln\left(\frac{p|O_2}{p\|O_2}\right) \qquad (10.2)$$

where, p/O_2 and $p//O_2$ represent the oxygen partial pressures on the opposite sides of YSZ electrolyte.

As it can be seen in Fig. 10.3, the current of the $La_{0.9}Sr_{0.1}YO_{3-\delta}$ cell initially increases and then a plateau is observed as the applied voltage value increases (U). At U>0.7V the limiting current is observed. At U>1.5V the current becomes dependent again on the applied voltage, mainly because of the electrolyte's partial decomposition. At the YSZ cell, ΔV_{OC} increases at a low rate at first and then increases at a higher rate because of the decrease of hydrogen content in the interior of the sensor.

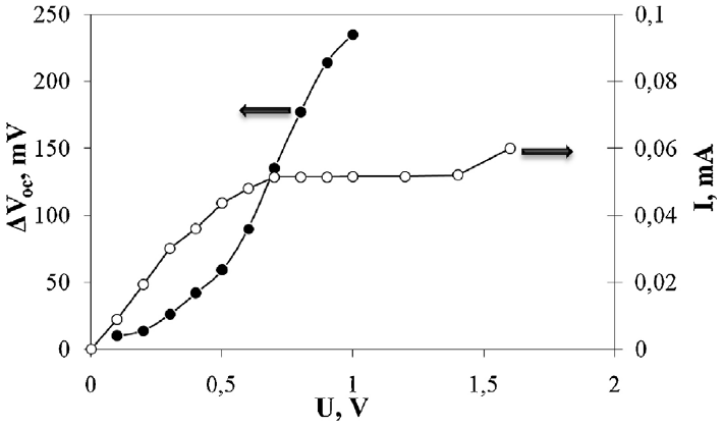

Figure 10.3. Current and open circuit electric potential difference of the sensor as functions of applied voltage for 0.7 vol. % H_2 + N_2 gas mixture at 550 ◦C [45].

In Fig. 10.4, it is shown that by increasing hydrogen content the voltage values at which the plateau is observed significantly grow. When 3% vol.H_2 is inserted into the sensor, the plateau begins to appear at the highest voltage value giving the optimal performance of the sensor.

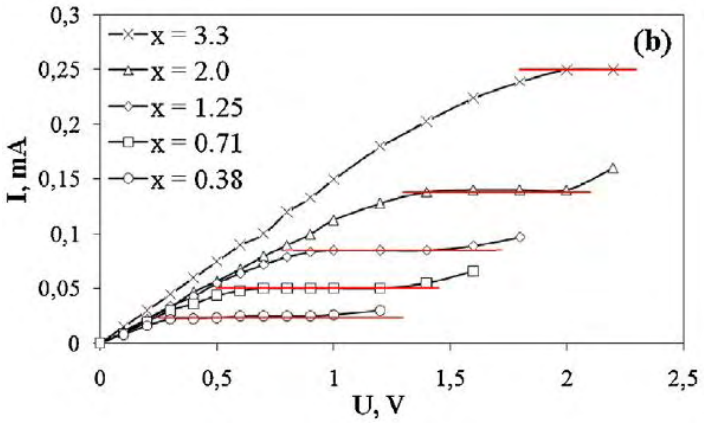

Figure 10.4 The dependences of current as a function of applied voltage at 550 ◦C for x vol.% H_2 + N_2 gas mixture at low (a) and relatively high (b) hydrogen concentration [45].

The strict linear function of the current response on the H_2 content indicates that the sensor is appropriate for the detection of low hydrogen concentration as well (Fig. 10.5).

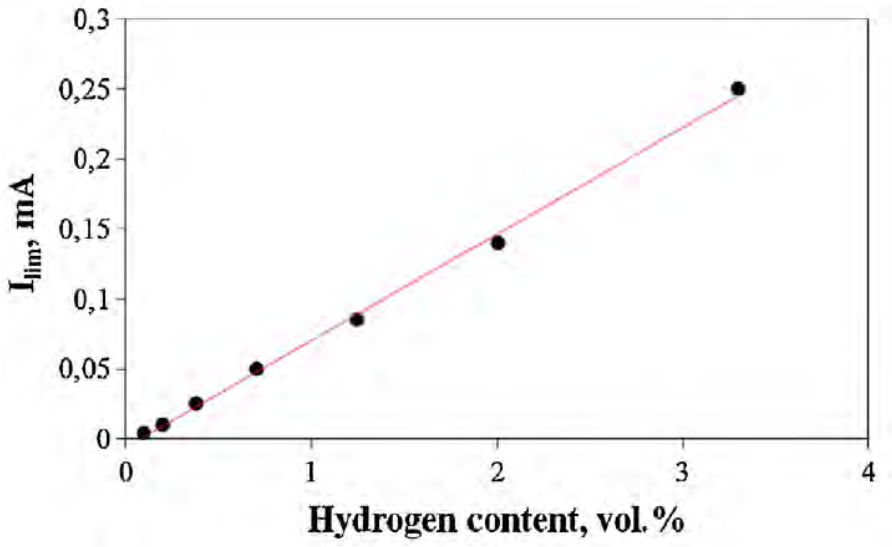

Figure 10.5. The limiting current dependence as a function of hydrogen content in x vol.% H_2+N_2 gas mixture at 550◦C [45].

The developed sensor displayed good detection capability even of small amounts of hydrogen (0.1-3.3 vol.%) in N_2 at 500-600ºC .

10.1.2 Combined amperometric and potentiometric sensor

Another type of intermediate-temperature sensor that has been investigated are combined amperometric and potentiometric hydrogen sensors based on $BaCe_{0.7}Zr_{0.1}Y_{0.2}O_{3-\delta}$ proton-conducting ceramic, studied by Tsiakaras *et al.* $BaCe_{0.7}Zr_{0.1}Y_{0.2}O_{3-\delta}$ (also known as BZCY), is a proton-conducting material which exhibits high ionic conductivity and acceptable stability in aggressive atmospheres (containing H_2O, CO_2 and H_2S in high temperatures. Investigations of proton-conducting materials applications for hydrogen detection are limited by the work of few scientific groups, even if they are regarded as perspective materials for sensory equipment. Ceramic materials allow expanding the temperature range of application such as the estimation of hydrogen partial pressure value in different gas mixtures and the determination of hydrogen concentration in steels and melts.

The developed sensor consists of two electrochemical cells, separated by a chamber and a capillary. The platinum electrodes are located on both sides of each cell, achieving good contact between the functional materials. The capillary and joints between the cells were sealed by high-temperature glass. The first cell (Cell 1) was used as an electrochemical hydrogen pump and the other one (Cell 2) worked in potentiometric

regime. The sensor operates in both amperometric and potentiometric modes based on the polarity of the applied voltage.

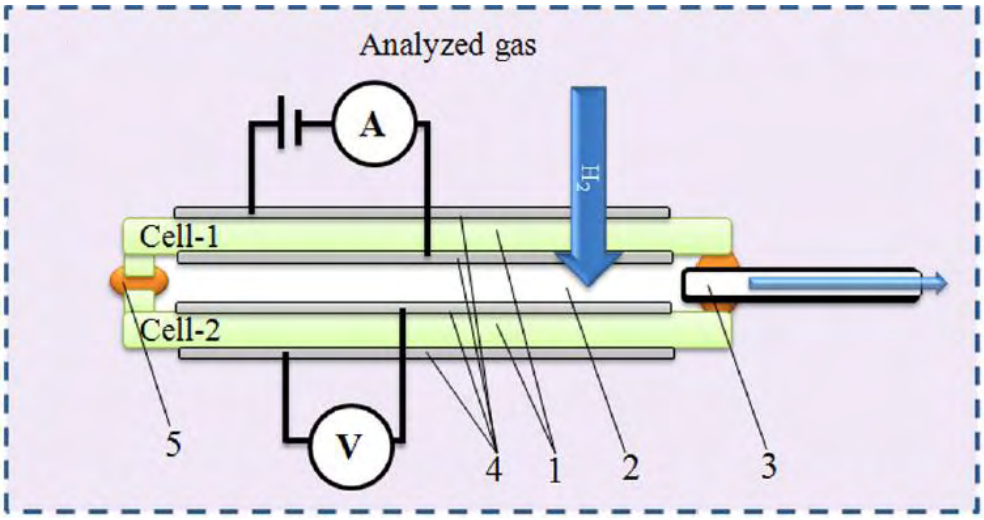

Figure 10.6. The scheme and the working principle of the developed sensor in potentiometric mode: 1—$BaCe_{0.7}Zr_{0.1}Y_{0.2}O_3$− electrolyte, 2—sensor's chamber, 3—diffusion channel (capillary), 4—platinum electrodes, 5—high-temperature glass sealant [50].

In the case of potentiometric regime (Fig. 10.6), a DC voltage (ΔU) is applied on the Cell 1 to provide the electrochemical pumping of hydrogen from the analyzed gas towards the internal chamber. The electrochemical reaction that takes place on the external electrode is:

$$H_2 \rightarrow 2H^+ + 2e^- \qquad (10.3)$$

The counter reaction of Eq. 10.3 is realized on the internal electrode of Cell 1. Thus, hydrogen permeates through the electrolyte in its ionic form. Hydrogen gradually replaces nitrogen in the chamber of the sensor, until a pure hydrogen atmosphere is created. An electric potential difference (E) is generated in Cell 2, due to the difference in hydrogen partial pressures between internal (//) and external (/) chambers of the sensor. The value of E is estimated according to the Nernst equation:

$$E = \frac{RT}{2F} \ln\left(\frac{p\|H_2}{p|H_2}\right) \qquad (10.4)$$

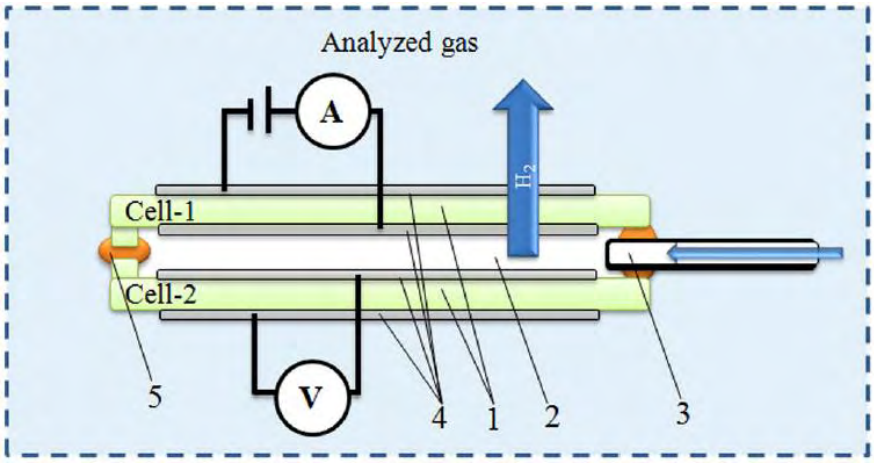

Figure 10.7. The scheme and the working principle of the developed sensor in amperometric mode: 1—$BaCe_{0.7}Zr_{0.1}Y_{0.2}O_3$− electrolyte, 2—sensor's chamber, 3—diffusion channel (capillary), 4—platinum electrodes, 5—high-temperature glass sealant [50].

In the case of amperometric mode, a voltage between the electrodes of Cell 1 is applied. This causes a hydrogen transfer from the interior space of the sensor to the external space, which is compensated by hydrogen flow permeating through the diffusion barrier from gas mixture. This way, an electrical current is produced to Faraday's law:

$$J(H_2) = \frac{I}{2F} \qquad (10.5)$$

The flow of hydrogen pumped out increases with increasing the voltage applied to the electrodes of Cell 1, until limiting current is observed. Thus, obtaining the $I_{lim}=f(pH_2)$ calibration curve, the amperometric mode of operation of the sensor can be used for hydrogen content detection.

The potentiometric mode of operation was suitable for analysis of gas mixtures with low-level hydrogen concentration due to the high hydrogen partial pressure difference, according to Eq. 10.4. The electrochemical characteristics were obtained depending on the change of T and pH_2. According to Fig. 10.8, the increasing ΔU causes an increase in pumping current.

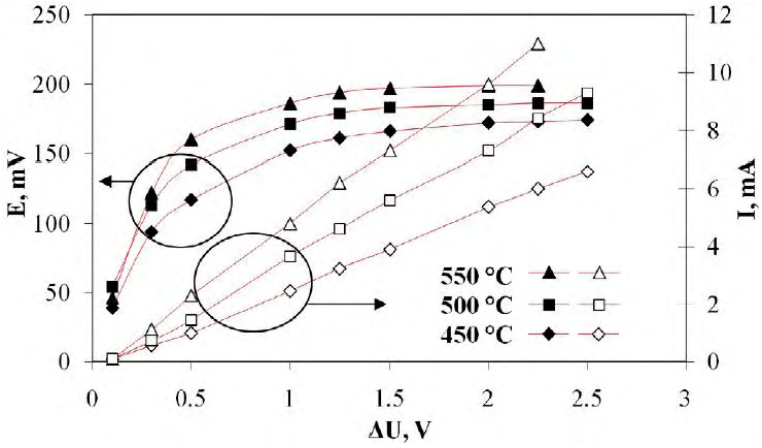

Figure 10.8. The pumping current and electric potential difference values depending on applied voltage and temperature for the sensor working in potentiometric mode in N_2+2%H_2O+0.4%H_2 atmosphere [50].

As it can be seen by Fig. 10.9, high hydrogen partial pressure difference created by Cell 1, leads to high values of E on Cell 2.

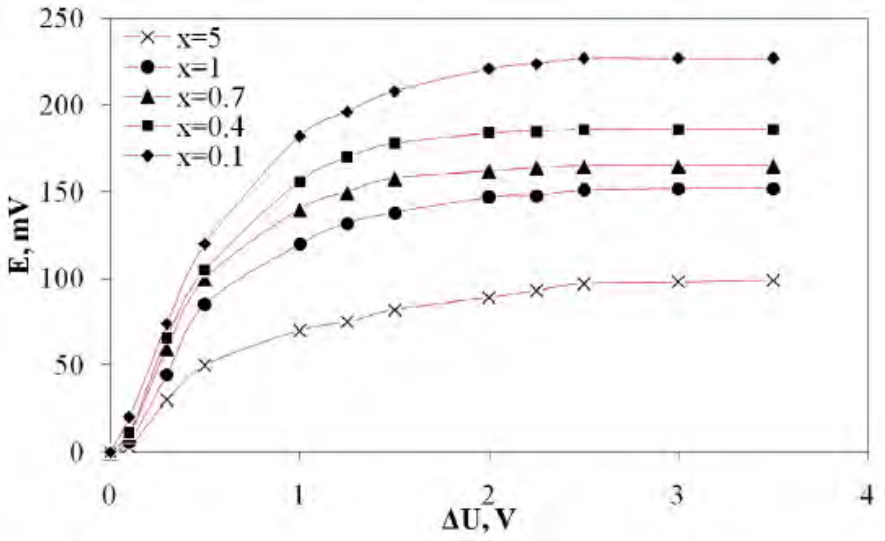

Figure 10.9. The electric potential difference values as a function of applied voltage for N_2+2%H_2O+x%H_2 gas mixture at 500◦C [50].

The amperometric mode of operation is suitable for the detection of relatively high concentrations of hydrogen. The current dependences on the applied voltage for the sensor during the amperometric operation is shown by Fig. 10.10 and Fig 10.11.

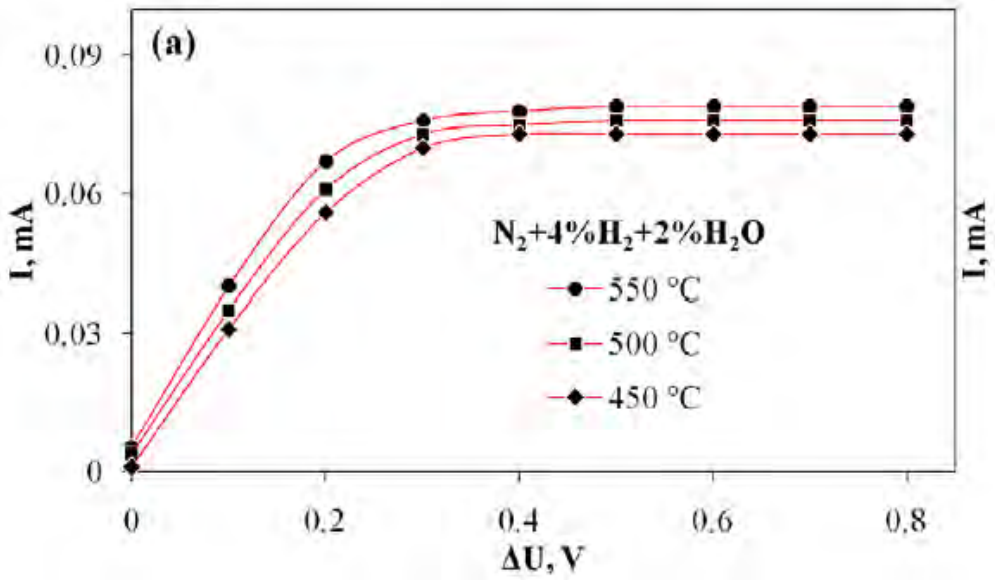

Figure 10.10. The current dependence on applied voltage at different temperatures in N_2+2%H_2O+x%H_2 gas mixture for the sensor working in amperometric mode [50].

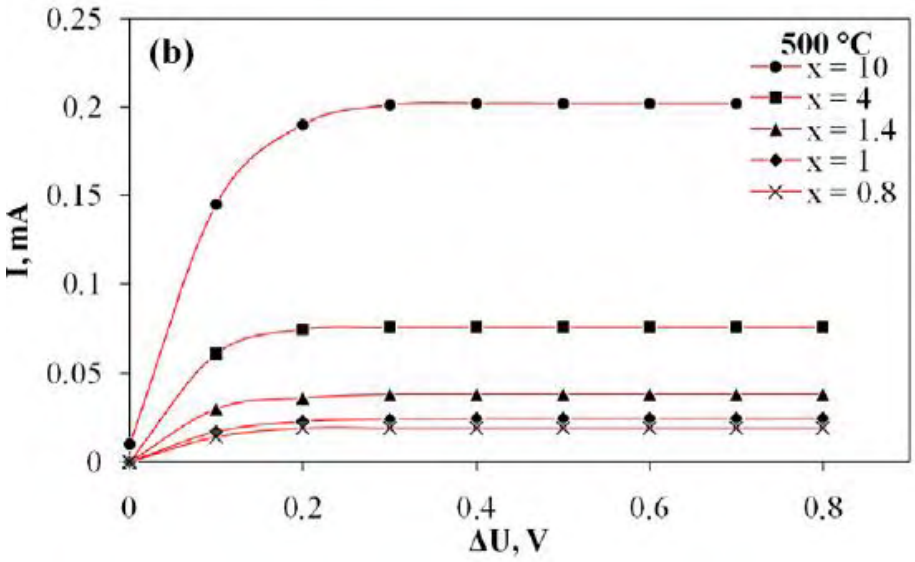

Figure 10.11. The current dependence on applied voltage at different hydrogen concentrations in N_2+2%H_2O+x%H_2 gas mixture for the sensor working in amperometric mode [50].

Applied voltage independence of the current is described by the limiting current determines the highest pumping-out rate of hydrogen under steady state conditions. As it is depicted by Fig. 10.10 and Fig. 10.11 the limiting current grows alongside with the rise of temperature and hydrogen concentration respectively.

According to the linear curve of Fig. 10.12, which obtained by the concentration dependence of the limiting current (Fig. 10.11), the measurement of hydrogen concentration is also possible by the amperometric mode of the developed sensor.

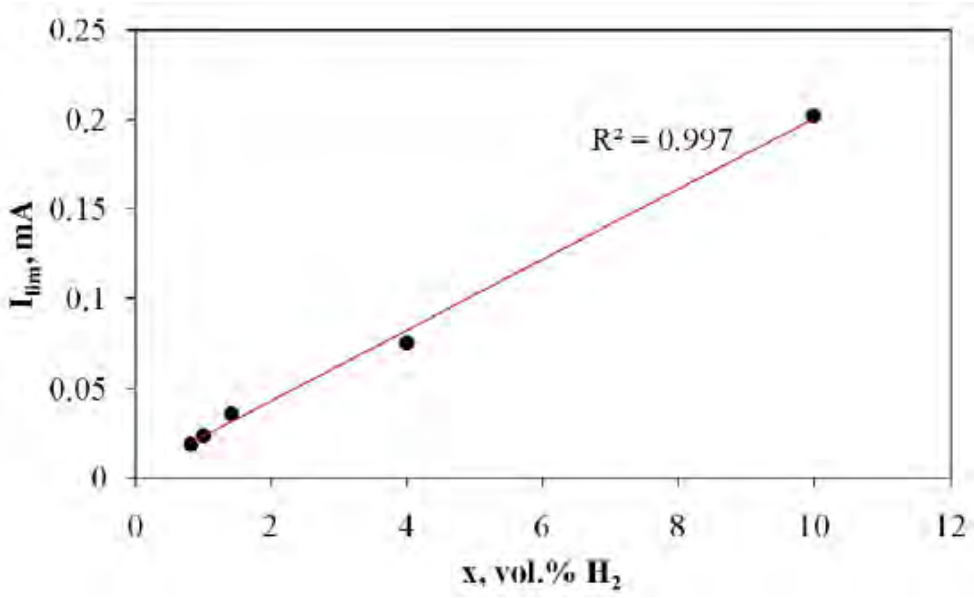

Figure 10.12. The limiting current as a function of hydrogen content in N_2+2%H_2O+x% H_2 gas mixture at 500◦C [50].

10.2 H_2, CO and CH_4 amperometric sensors

The most common and one of the most reliable and stable sensors for automotive industries is potentiometric λ-sensor, based on yttria-stabilized zirconia (YSZ). YSZ is characterized by both chemical and mechanical stability, relatively high oxygen ion conductivity and good adhesive behavior over a long period of time. However, the major disadvantages of potentiometric YSZ sensors are difficulties that they display regarding the establishment of a reference atmosphere and where the Nernst potential for an analyzed gas component does not exist. For this reason, amperometric sensors have been designed as well. They appear as a possible solution to the above drawbacks of potentiometric sensors. Some of the most widely investigated amperometric sensors are used for the detection of medium and high oxygen concentration and YSZ sensors for the detection of NO_x in automotive exhausts [51].

Thus far, amperometric sensors based on oxygen-conducting solid electrolytes for monitoring combustible gases in inert gas media, have not been widely studied. The measurement of combustible gases in their mixtures with nitrogen is appealing, because most common thermal catalytic analyzers cannot be used for the analysis of combustible gases in oxygen-free media. Tsiakaras *et al.* have recently investigated an amperometric sensor based on 9YSZ solid electrolyte (0.91 ZrO_2 + 0.09Y_2O_3), with a metal capillary for the detection of hydrogen, carbon monoxide and methane in nitrogen atmospheres [51] .

The sensor is composed of a chamber connected by a diffusion barrier with an outer space. The diffusion barrier was made of metallic capillary. Electrodes are located on the interior and outer surface of the chamber wall. The scheme of the sensor can be seen in Fig. 10.13 [51].

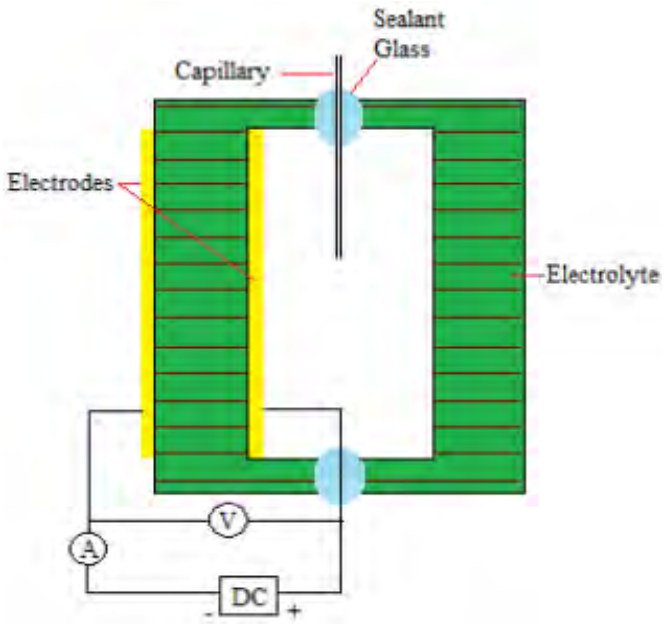

Figure 10.13. Schematic representation of an amperometric sensor.

DC voltage is applied to the electrodes so that the concentration of the analyzed component inside the chamber decreases; therefore, a positive potential is applied to the inner electrode. Thus, decomposition of steam or carbon dioxide occurs at the outer electrode [51]:

$$H_2O + 2e^- \rightarrow H_2 + O^{2-} \qquad (10.6)$$

$$CO_2 + 2e^- \rightarrow CO + O^{2-} \qquad (10.7)$$

The first reaction occurs because steam exists in the analyzed gas due to residual humidity (~10ppm) in nitrogen and due to oxidation of hydrogen by traces of oxygen (~10ppm) in nitrogen. For the second reaction, carbon dioxide exists in the mixture N_2+CO and N_2+CH_4 because of oxidation of combustible gases by traces of oxygen in nitrogen. Oxygen ions pass through the YSZ electrolyte into the chamber. They oxidize hydrogen at the internal electrode [51]:

$$H_2 + O^{2-} \rightarrow H_2O + 2e^- \qquad (10.8)$$

The operation of the sensor is similar in the case of other combustible gases such as CO and CH_4 in nitrogen. The respective reaction at the internal electrode are [51]:

$$CO + O^{2-} \rightarrow CO_2 + 2e^- \qquad (10.9)$$

$$CH_4 + 4O^{2-} \rightarrow CO_2 + 2H_2O + 8e^- \qquad (10.10)$$

The lower concentration of the combustible component inside the sensors chamber under the applied voltage secures the constant diffusion of flux of combustible gas. The equation for the limiting diffusion flux of the "k"-component (k=H_2, CO and CH_4), which occurs under the limiting current, $J_{k,lim}$, in the capillary is [51]:

$$J_{k,lim} = \frac{C_k D_k S}{L} \quad , \qquad (10.11)$$

where S is the cross section area and L the length of the capillary. The corresponding limiting current is estimated by:

$$I_{k,lim} = z_k D_k X_k \frac{PFS}{LRT} \qquad (10.12)$$

where P is the total pressure of the analyzed gas.

The dependence of the applied voltage and the sensor current for various gas mixtures of the aforementioned combustible gases and nitrogen at 450^{o}C is shown in Figs 10.14-10.17 [51].

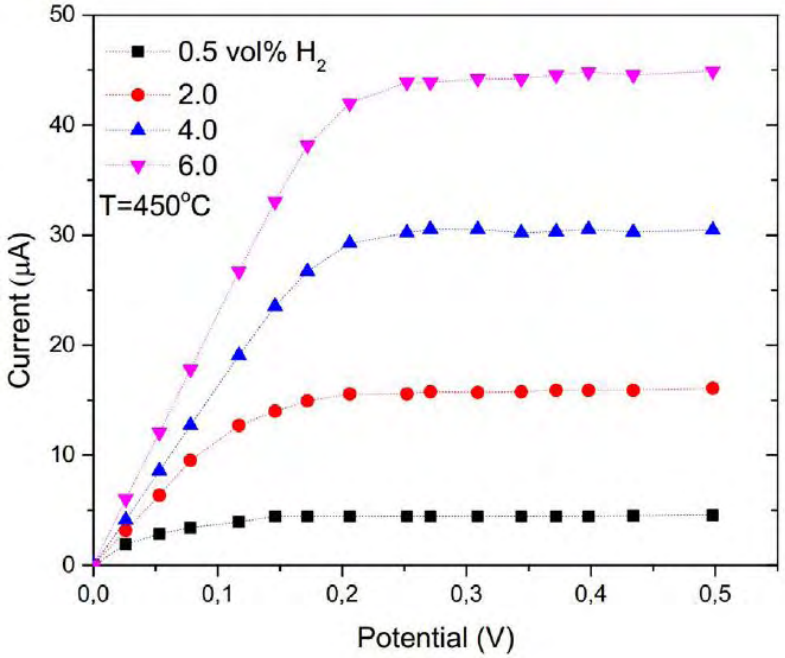

Figure 10.14. Volt–ampere characteristic curves of the sensor fed with N_2+H_2 mixtures [51].

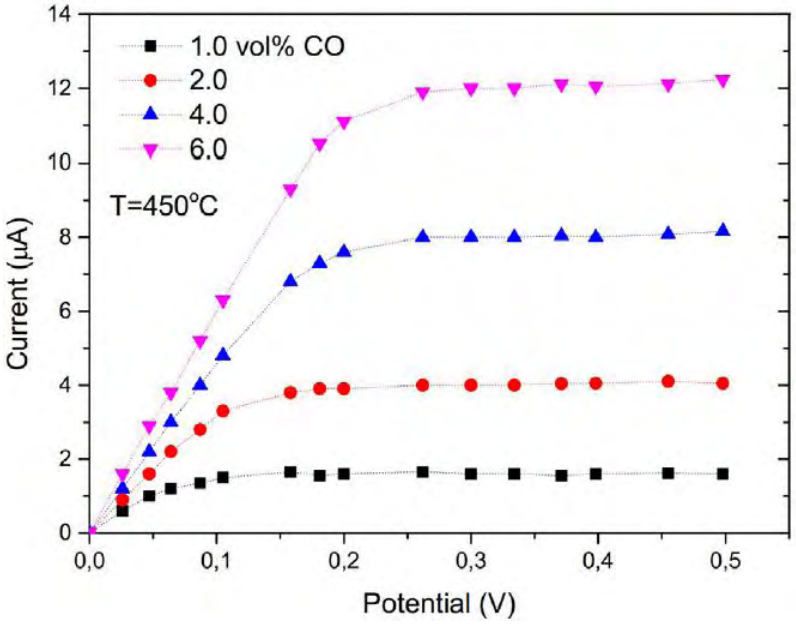

Figure 10.15. Volt–ampere characteristic curves of the sensor fed with N_2+CO mixtures [51].

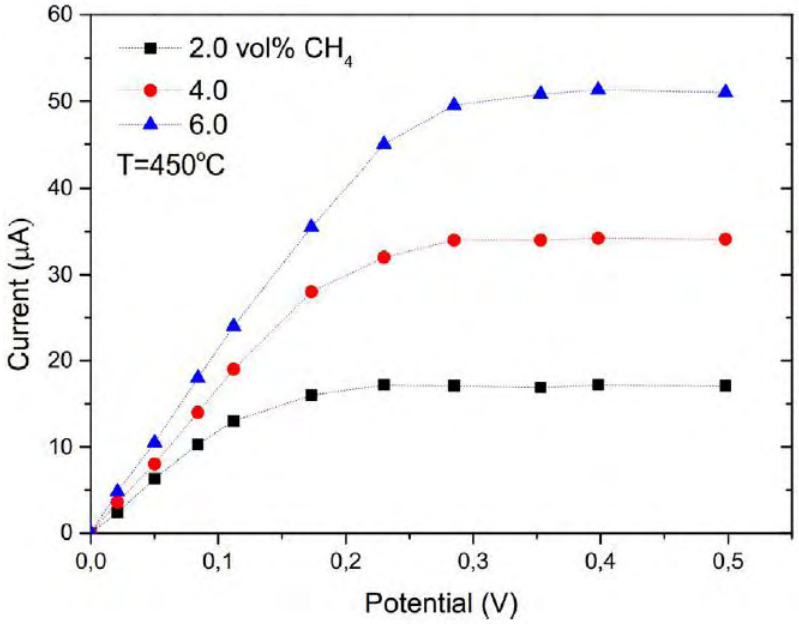

Figure 10.16. Volt-ampere characteristic curves of the sensor fed with N_2+ CH_4 mixtures [51].

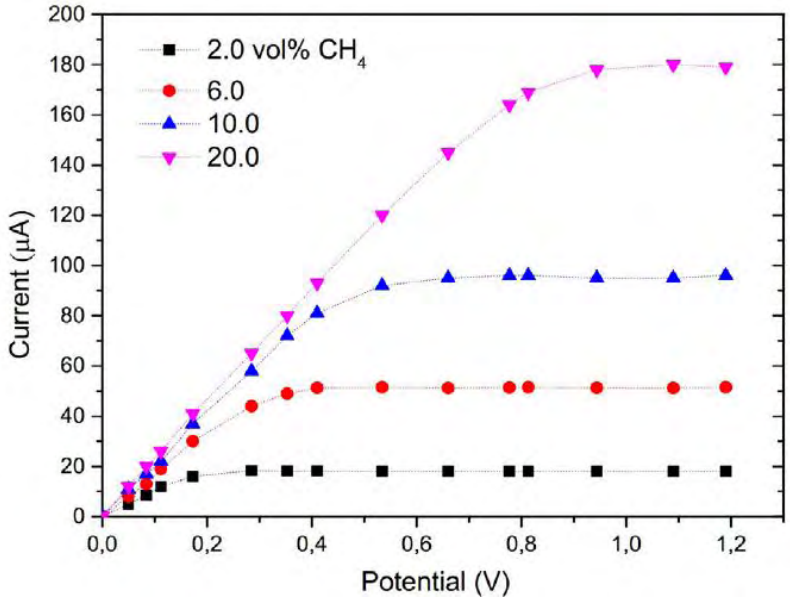

Figure 10.17. Volt–ampere characteristic curve of the sensor fed with N_2+CH_4 mixture in a wide range of CH_4 concentration [51].

It is observed that for all mixtures the I-V curve slope decreases with the decrease in the concentration of the component. The initial part of the I-V curves exhibit different slopes, which represent the characteristics of total internal resistance of each sensor. The latter part includes Ohmic resistance of the electrolyte and polarization resistances of the external and internal electrodes. The main impact of the electrolyte's resistance to the total resistance gives the electrode's polarization resistance. The lower the total resistance the easier it is for the electrochemical reactions 10.8-10.10 to take place.

Furthermore, the diffusion rate of each combustible in N_2 affects the I-V behavior and more specifically the limiting current [51].

It is shown by Fig. 10.18, that for all examined combustible gases, the dependence of the limiting current on the gas content in N_2 display approximately linear behavior [51].

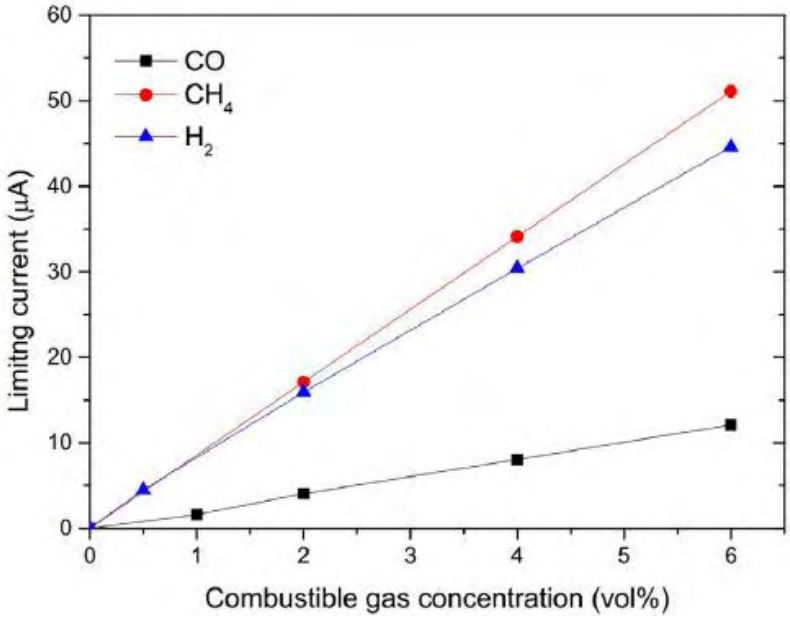

Figure 10.18. Dependence of sensor limiting current on combustible gas concentration [51].

In addition, by the aid of Eq. 10.12 and Fig. 10.18, the following expression for the diffusion coefficient can be obtained [51]:

$$D_k = \frac{I_{k,lim}}{X_k} \cdot \frac{LTR}{z_k PSF} \qquad (10.13)$$

10.3 Oxygen and humidity sensors

As it has been mentioned above, electrochemical sensors based on YSZ have been proved to be robust and highly reliable. However, bulk YSZ oxygen sensors have limited applications because of their demand of large amounts of energy, since they require to be heated to 400°C to function properly. Also, handling objects at such temperatures is an obstacle. For these reasons, micro-electrical-mechanical-system (MEMS)-processed microheaters have been used in order to decrease the energy requirements and size of the sensor. It has been applied on methane, hydrogen sulfide and carbon oxide sensors [52].

Nevertheless, no electrochemical oxygen sensors based on YSZ have been widely investigated. The main reason are difficulties in the fabrication of thin film YSZ-based sensor on a silicon substrate. This type of sensors require a porous Pt anode and cathode, an YSZ electrolyte and a gas diffusion layer. All parts of the sensor should be made of

thin films on silicon substrates, for the incorporation of the sensor onto a microheater. Akasaka has proposed a thin film YSZ amperometric oxygen and humidity sensor, installed onto a microheater [52].

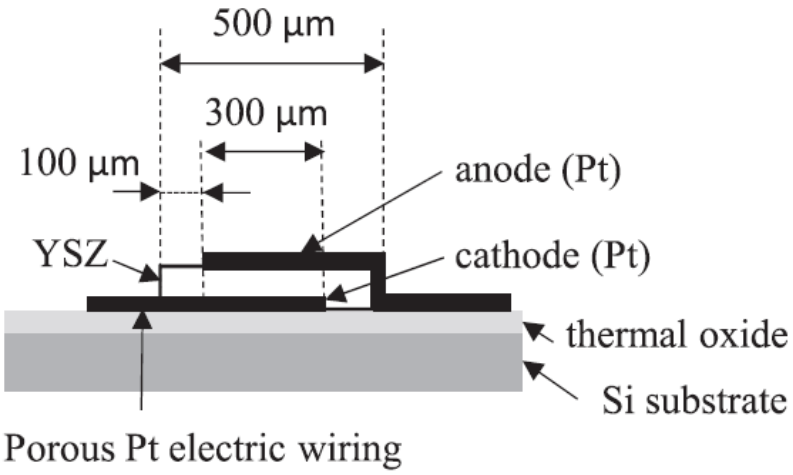

Figure 10.19. Structure of limiting current-type sensor, fabricated on a silicon substrate [52].

The porous Pt cathode and wiring as a catalyst and a gas diffusion layer as well. The determination of limiting current depends on the gas diffusion through this layer. The size of the pathway affects the diffusion of gas to the sensor; therefore, the cross-sectional area of the porous Pt wiring that connects the Pt cathode Pt pad electrode is important [52].

Fig. 10.20 demonstrates the current-voltage dependence between 400-550^{o}C. It is observed that two plateau stages are formed in this temperature range [52].

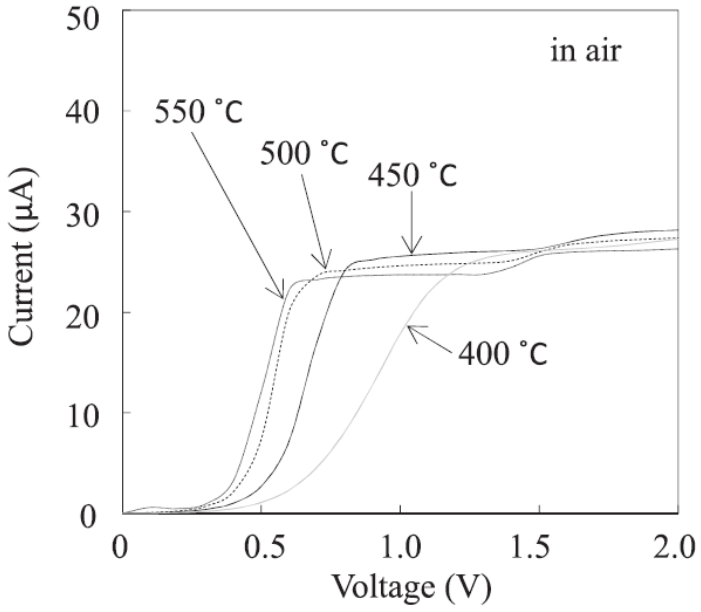

Figure 10.20. Voltage-current characteristics between 400◦C and 550◦C in air [52].

Fig. 10.21 shows the oxygen concentration dependence of the current-voltage characteristics at 500°C, in a range of different concentrations.

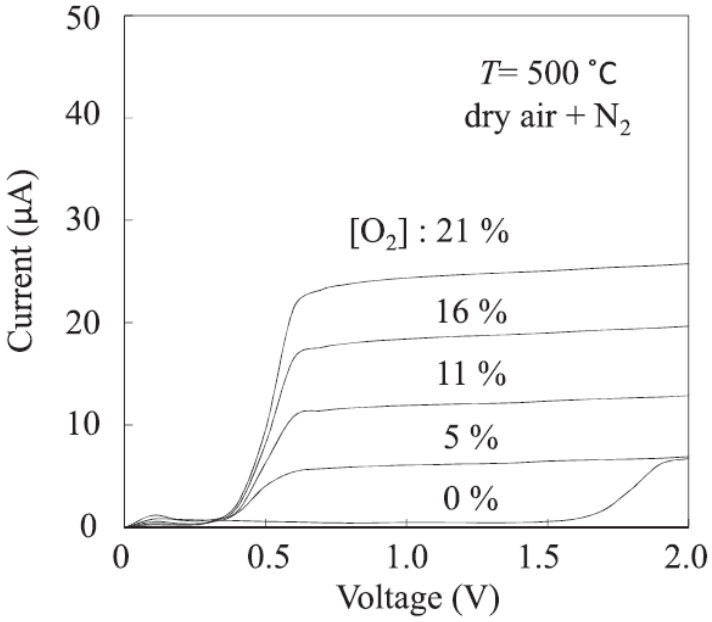

Figure 10.21. Oxygen concentration dependence of voltage-current characteristics at a temperature of 500◦C, under a mixture of dry air and N2 [52].

The oxygen concentration in air is 21%. It is observed that the curve for this concentration at 500°C in Fig. 10.21 is the same with the curve of Fig. 10.20 for 500°C, until the end of the first plateau. Consequently, it is conducted that the current plateaus at the lower and higher voltage regions correspond to the reduction of oxygen and water vapor, respectively. The reduction of PtO_x, which is formed at the interface between the Pt cathode and YSZ film is the reason that current peaks appear in Fig. 10.21 [52].

As it can be seen by Fig. 10.22, there is a linear relationship between the oxygen concentration and the limiting current. This indicated that the porous Pt is sufficiently efficient as a gas diffusion layer [52].

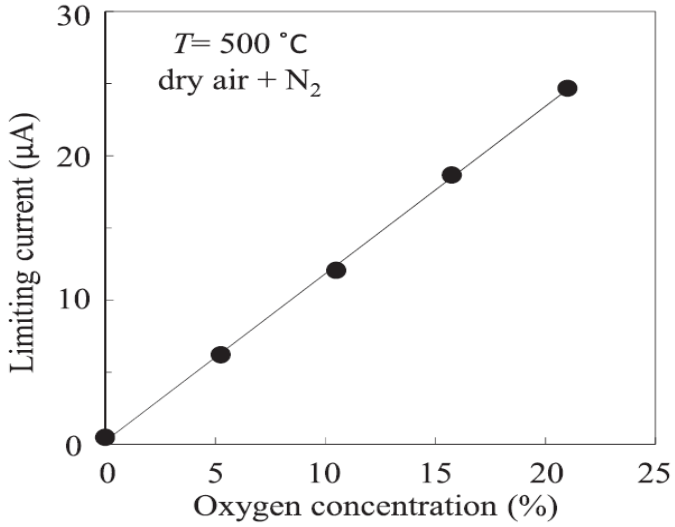

Figure 10.22. Relationship between oxygen concentration and limiting current at a temperature of 500°C, under a mixture of dry air and N_2 [52].

Fig 10.23 shows the water vapor pressure dependence of the current-voltage characteristics at 500°C. The control of water vapor pressure was achieved by alternating the flux rate of dry and wet air [52].

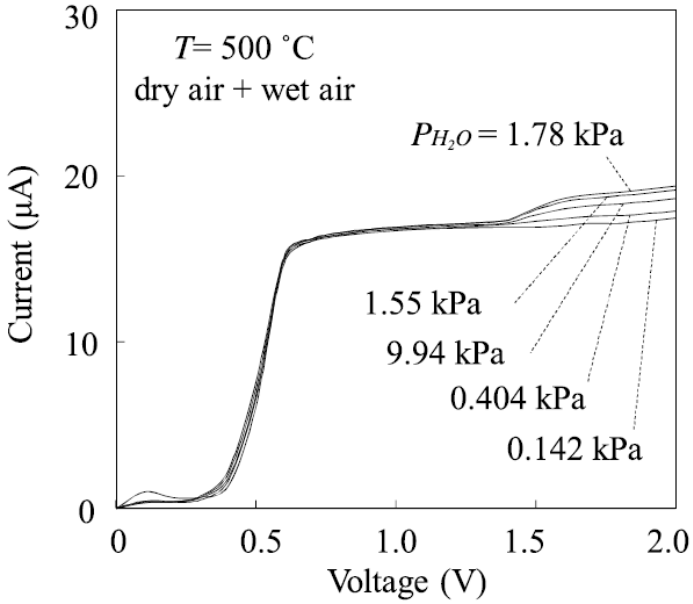

Figure 10.23. Water vapor pressure dependence of voltage-current characteristics at a temperature of 500°C, under a mixture of dry air and wet air [52].

The limiting current at the lower and higher applied voltage regions are affected by the oxygen concentration and the water vapor pressure. A linear relationship between water vapor pressure and the limiting current was observed at 1.8V. However, no distinct correlation was observed at 1.1V, as show in Fig. 10.24 [52].

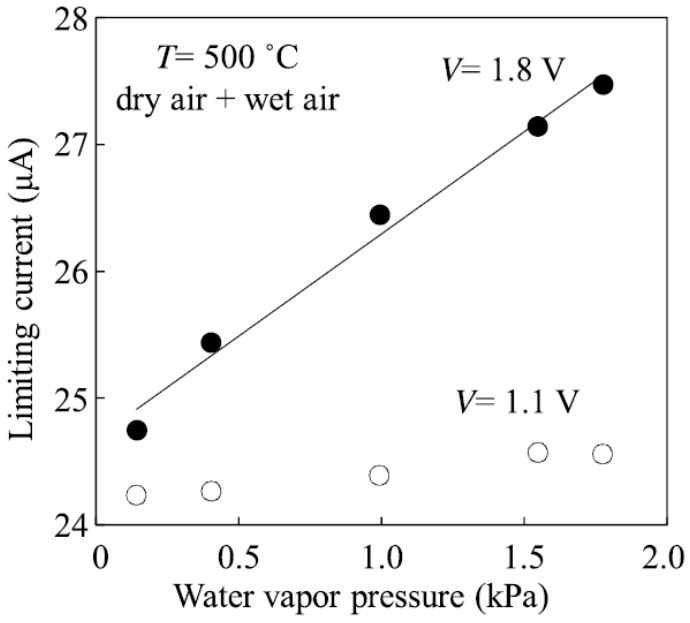

Figure 10.24. Relationship between water vapor pressure and limiting current at 1.1 V(open circles) and 1.8 V (closed circles) at a temperature of 500°C, under a mixture of dry air and wet air [52].

The above results indicate that both the oxygen concentration and the water vapor pressure can be calculated by the as proposed sensor. It is expected that the use of a microheater will reduce the energy consumption of amperometric oxygen and humidity electrochemical sensors [52].

CHAPTER 11: NH_3 ELECTROCHEMICAL SENSOR

Abstract

In the present chapter, the fabrication and characterization of an ammonia electrochemical sensor, based on oxygen ion solid electrolyte, is presented. The results that are reported allows one to conclude that this simple amperometric sensor can be considered as a useful tool for gas analysis and measuring the gas diffusion coefficients as well.

11.1 Introduction

Solid electrolytes based on zirconium oxide have a wide range of applications in many scientific and technologic sectors. Oxygen and hydrogen amperometric sensors for the detection of high, average and low concentrations of the analyzed component are widespread and some of them are reported above [53-57] .

Solid electrolyte amperometric sensors, for the detection of H_2, C_2H_5OH, N_2O in inert gas environment, based on $0.91ZrO_2+0.09Y_2O_3$ are well known [58-63]. Recently, solid electrolytes with proton conductivity are regarded as prospect materials for applications in both amperometric and potentiometric solid electrolyte gas sensors [44, 45, 50].

Currently, there is no information in literature for the use of amperometric sensors, based on oxygen ion or proton-conducting electrolyte, for monitoring of ammonia. In practical cases, measurement of the ammonia concentration in mixture with nitrogen is important. Such sensors can find applications in technology of production of ammonia, nitrogen fertilizers, explosives, polymers, nitric acid, soda (by an ammoniac method) and other products of chemical industry.

An amperometric sensor based on oxygen ion solid electrolyte for the measurement of ammonia was fabricated and tested in the present work. The sensor was composed of two electrochemical cells separated by a gas chamber and a capillary connecting the sensor chamber to the analyzed atmosphere. The development procedure and experimental results are presented below.

11.2 Operation principle

As it can be seen in Fig. 11.1, the amperometric sensor is composed of two electrochemical cells and a capillary. Each cell is made of a square plate from 9YSZ electrolyte with a recess from one side. Platinum electrodes are located on both sides of the square plate. Also, the plates are piled in such way so that an internal cavity is formed and are glued perimetrically by a sealant.

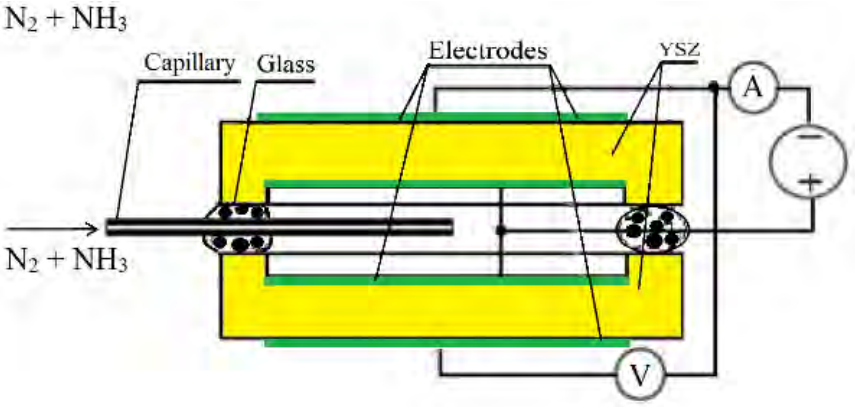

Figure 11.1. Scheme of an amperometric sensor.

After its fabrication, the sensor is put in the NH_3-N_2 mixture. The content of impurities in this mixture (mainly H_2O) is lower than 0.1 vol. %. After that, a DC voltage is applied to the external electrodes. There, the decomposition of steam occurs:

$$H_2O + 2e^- \rightarrow H_2 + O^{2-} \qquad (11.1)$$

Oxygen ions are transferred through the electrolyte to the internal chamber of the cell. Electrochemical oxidation of ammonia takes places at the internal electrodes. Catalytic oxidation of ammonia can lead to formation of molecular nitrogen and nitrogen oxides [64].

$$NH_3 + 0.75O_2 \rightarrow 0.5N_2 + 1.5H_2O \qquad (11.2)$$
$$NH_3 + O_2 \rightarrow 0.5N_2O + 1.5H_2O \qquad (11.3)$$
$$NH_3 + 1.25O_2 \rightarrow NO + 1.5H_2O \qquad (11.4)$$

The corresponding electrochemical reactions are:

$$NH_3 + 1.5O^{2-} \rightarrow 0.5N_2 + 1.5H_2O + 3e^- \qquad (11.2a)$$
$$NH_3 + 2O^{2-} \rightarrow 0.5N_2O + 1.5H_2O + 4e^- \qquad (11.3a)$$
$$NH_3 + 2.5O^{2-} \rightarrow 0.5NO + 1.5H_2O + 5e^- \qquad (11.4a)$$

As the applied voltage gradually rises, there is a gradual increase in the current too. The ammonia content in the sensor decreases and the ammonia diffusion flux into the sensor cavity increases; after that, a certain constant value is reached. This value is the

limiting current (I_{lim}). It meets the conditions of zero content of ammonia in the interior of the sensor, which diffuses from the external environment to the internal chamber through the capillary. I_{lim} is related to environmental parameters, the capillary's dimensional parameters and the analyzed component concentration:

$$I_{lim} = \frac{zFDSP}{RTL} \cdot X \qquad (11.5)$$

Where F is the Faraday's constant, R is the universal gas constant, D is the diffusion coefficient of ammonia in nitrogen, P is the total pressure, T is absolute temperature, S and L are the capillary's cross section area and length, X is the mole fraction of ammonia and z is the number of electrons participating in the electrochemical reaction: z=3, 4, 5 for electrochemical reactions 11.2a-11.4a respectively.

According to Eq. 11.5, the limiting current in the mixture ammonia+nitrogen is directly proportional to a molar fraction of ammonia. It is also affected by temperature and type of electrochemical reaction.

When the applied voltage reaches high values, the sensor current exceeds the limiting current. Then, oxygen is formed in the sensor chamber, according to the following reaction which occurs at the internal electrode:

$$O^{2-} \rightarrow 0.5O_2 + 2e^- \qquad (11.6)$$

The voltage applied to the sensor when the sensor current begins to grow has to exceed the voltage corresponding to the beginning of the limiting current plateau by the EMF of an electrochemical chain:

$$O_2(p_{O_2})|O^{2-}|H_2O(p_{H_2O}) \qquad (11.7)$$

At the sensor operating temperatures, the EMF value equals several hundreds of millivolts. As voltage further increases, the sensor current rises because of the reaction 11.6 and is not related to the diffusion limitation.

11.3 Experimental

The dimensions of the electrochemical cells which are demonstrated in Fig. 11.1 are 11 x 11mm and the thickness is 1mm. The depth of the recess is 0.5mm with an area of 60mm^2. The platinum electrodes were placed on the opposite sides of each electrolyte plate. The platinum wires were connected to the electrodes and painted by a platinum paste so that a sufficient conjunction is reached between wires and electrodes after a treatment at 1100^{o}C for 1h. The interior space of the electrochemical cell is formed by the aid of the prepared plates. This is achieved with a high-temperature gluing, using a high-temperature sealant. A thin-walled chromo-nickel steel capillary with an internal

diameter of 160μm and a length of 22mm was sealed between the plates allowing connection between the interior and outer gas spaces of the sensor.

The amperometric sensor was placed in the tubular furnace and heated up to standard temperatures in a range of 375-430°C. The temperature was held at a constant value with an accuracy of ±1°C. The calibrated N_2+NH_3 gas mixture with a content of 1-5 vol. % NH_3 and a flow rate of 50ml/min was supplied to the tubular furnace. Mass flow controllers of F-201C-33-V type were utilized for required gas mixtures preparation. The V-I measurements were achieved after reaching the equilibrium between the internal and external spaces of the sensor; under open circuit voltage condition, potential difference was close to zero. GPS-18500 direct current source was used for applying the voltage to the sensor. The values of current and voltage were measured by the aid of MNIPI V-7-77 multimeters.

11.4 Results and Discussion

Fig. 11.2 shows the volt-ampere relationship of the sensor's current operating in different N_2+NH_3 environments. Each curve is related to a certain ammonia content and consists of three well-distinguished areas. At the first area, the current increases alongside with the applied voltage growth. The second area is related to the emergence of limiting current, which is indicated by the formation of a plateau on V-I curve. The last area, shows that the current increases with the increase of the applied voltage, which is explained by free oxygen appearance in the interior space of the sensor. It is observed that by altering the ammonia concentration, the shape of curves changes shifting the limiting current regions to the higher applied voltage values. The plateau area appears when the voltage reaches a value of 0.9-1.1V. It is also shown, that the extent of the plateau is of about 0.4-0.5V for each NH_3 concentration curve.

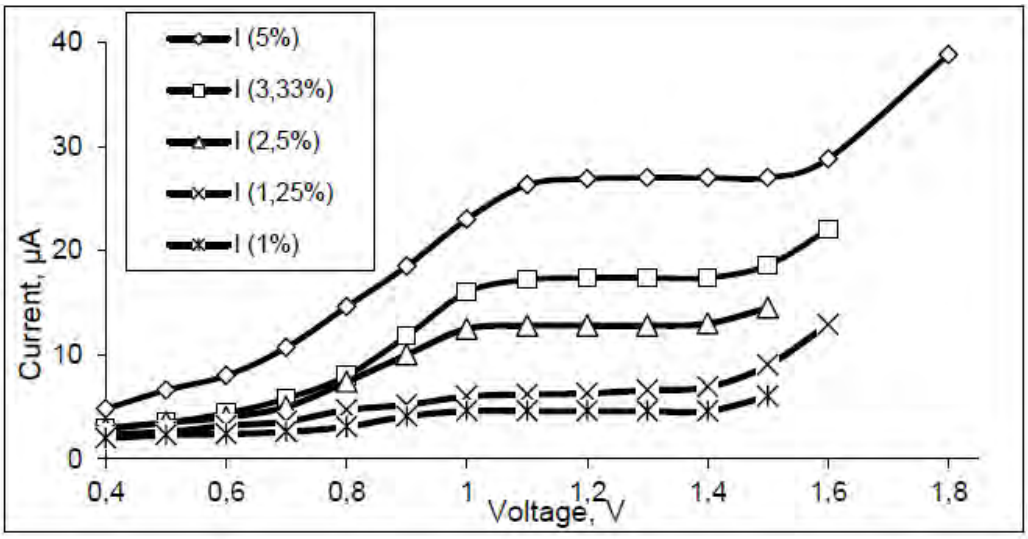

Figure 11.2. Dependences of a sensor current on voltage at different NH_3 concentration, temperature 400°C.

The most important concentration obtained from a number of the volt-ampere curves is the concentration dependence of the limiting current (μA) under isothermal conditions. This function, according to Eq. 11.5, should exhibit a linear behavior, which is confirmed by Fig. 11.3:

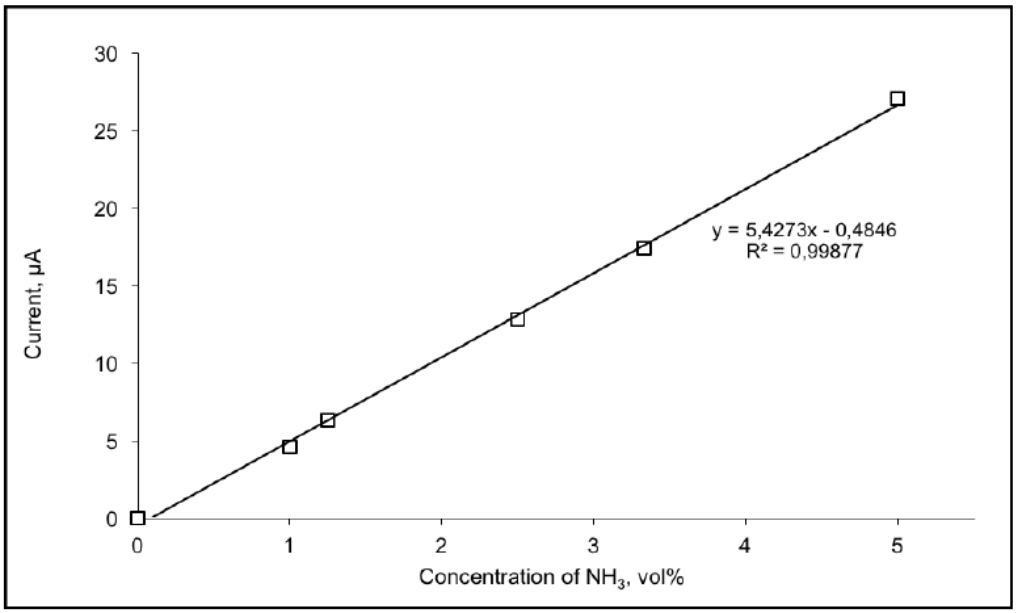

Figure 11.3. Dependence of a sensor limiting current on NH_3 concentration, temperature 400°C.

The effect of temperature on the volt-ampere behavior for the as developed sensor is observed in Fig. 11.4:

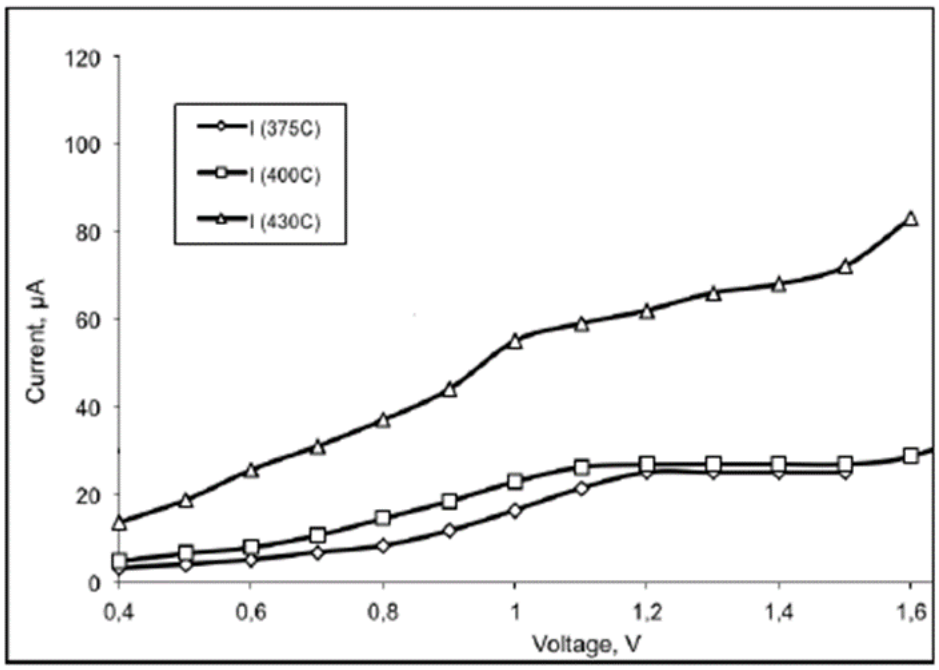

Figure 11.4. Dependences of a sensor current on voltage at various temperatures, concentration of NH_3 is 5%.

At relatively low temperatures, the appearance of a plateau can be clearly observed, whereas no limiting current region appears at higher temperature values. The slope of these dependences increases as the temperature increases as well. This growth is partially due to the decrease of the internal resistance of the electrochemical cells. Nevertheless, such a considerable increase cannot be explained by just the aforementioned reason. It is possible that at such high temperature as 430ºC, the partial catalytic ammonia decomposition takes place on the internal surface of the chromo-nickel steel capillary:

$$NH_3 \rightarrow 0.5N_2 + 1.5H_2 \qquad (11.7)$$

According to the above reaction, hydrogen is formed, which diffuses through the capillary to the interior of the sensor and then reacts with the oxygen ion:

$$H_2 + O^{2-} \rightarrow H_2O + 2e^- \qquad (11.8)$$

The diffusion coefficient of hydrogen in N_2 is approximately three times higher than that of ammonia. The number of electrons required for the electrochemical oxidation of the hydrogen which is formed according to reaction 11.7, is the same as for the electrochemical oxidation of NH_3, according to reaction 11.2a. Consequently, the hydrogen diffusion flow is higher compared to the ammonia diffusion flow and therefore the current should also be higher.

It is possible that only a part of ammonia decomposes according to reaction 11.7 and two diffusion flows –of ammonia and hydrogen- appear in the channel. Absence of the limiting current can occur by increasing the partial hydrogen diffusion flow alongside with a growth in the applied voltage; however, the nature of such behavior is unclear.

In addition, it is possible to specify the chemical essence of the electrochemical procedure and to define the type of the ammonia oxidation reaction. This is achieved by comparing the experimental and theoretical values of the mutual diffusion coefficients of N_2+NH_3 gas mixture. The experimental diffusion coefficients were defined by the aid of Eq. 11.5 by fitting the z parameter, while other ones are considered to be constant. The theoretical values of diffusion coefficients were estimated taking into consideration the molecular gas diffusion theory [65]:

$$D_{th} = \frac{0.001858T^{1.5}}{P\sigma^2\Omega_{DT}}\sqrt{\frac{1}{M_{N_2}} + \frac{1}{M_{NH_3}}} \qquad (11.9)$$

Where D_{th} is the theoretical diffusion coefficient (cm^2/s), T is the absolute temperature, P is the total pressure (bars), σ is the characteristic distance for ammonia+nitrogen mixture (Å), M_{NH_3} and M_{N_2} is the molecular mass of ammonia and nitrogen respectively, Ω_{DT} is the collision integral for diffusion. It depends on temperature according to the following equation:

$$\Omega_{DT} = \frac{A\varepsilon^B}{T^{-B}} + \mathrm{C}\exp\left(\frac{-DT}{\varepsilon}\right) + E\exp\left(\frac{-FT}{\varepsilon}\right) + G\exp\left(\frac{-HT}{\varepsilon}\right) \qquad (11.10)$$

where A=1.06036, B=0.1561, C=0.193, D=0.47635, E=1.03587, F=1.52996, G=1.76474, H=3.89411 and

$$\varepsilon = \frac{\varepsilon_{NH_3-N_2}}{k} = \frac{(\varepsilon_{NH_3}\varepsilon_{N_2})^{0.5}}{k} = \left(\frac{\varepsilon_{NH_3}}{k} \cdot \frac{\varepsilon_{N_2}}{k}\right)^{0.5} \quad (11.11)$$

Where $\varepsilon_{NH_3-N_2}$ is the characteristic energy for ammonia+nitrogen mixture, ε_{NH_3} and ε_{N_2} are the characteristic energies for ammonia and nitrogen respectively, while k is the Boltzmann's constant. According to [66]: $\frac{\varepsilon_{NH_3}}{k}$ =558.3K and $\frac{\varepsilon_{N_2}}{k}$ =71.4K. Using Eq. 11.9, the theoretical diffusion coefficient at temperature T can be calculated, if the diffusion coefficient at the standard conditions (T_o,Po) is known:

$$D_{th,T} = D_o \left(\frac{T}{T_0}\right)^{1.5} \frac{\Omega_{D_0}}{\Omega_{D_T}} \quad (11.12)$$

Where D_O is the diffusion coefficient at the standard conditions. Eq. 11.12 can be simplified to:

$$D_{th,T} = D_o \left(\frac{T}{T_0}\right)^{n} \quad (11.13)$$

Where n is the coefficient which can be found by calculation from theoretical model and from experimental data by using the following equation:

$$n = \frac{\log(\frac{D_T}{D_o})}{\log(\frac{T}{T_o})} \quad (11.14)$$

The n coefficient depends on the nature of gas mixture and it varies between 1.5 and 2 [44].

The experimental and theoretical data are presented in Table 11.1. These data are the diffusion coefficients (D), standard deviation (s) and n parameter values of the possible reactions for the electrochemical ammonia oxidation. (Eq. 11.2a-11.4a). As it is shown by the comparative analysis of D and n parameters, the product of electrochemical ammonia oxidations is N_2 rather than N_2O or NO, under the sensor operating conditions. The obtained results display good agreement with the literature data [64].

Table 11.1. Experimental and theoretical parameters of ammonia diffusion in nitrogen. $\Delta D/D_{th}$ and $\Delta n/n_{th}$ represent the relative differences between determined and calculated values. D_o=0.214m^2/s.

T, °C	equation	$D_{ex}\cdot10^4$,M^2/C	$s\cdot10^4$, M^2/C	$D_{th}\cdot10^4$, M^2/c	$\Delta D/D_{th}$, %	n_{ex}	n_{th}	$\Delta n/n_{th}$, %
400	(10.2a)	1.11	0.025	1.12	0.9	1.83	1.84	0.5
	(10.3a)	0.83	0.02		26	1.5		18
	(10.4a)	0.67	0.015		40	1.26		31
375	(10.2a)	1.01	0.034	1.05	3.8	1.79		3
	(10.3a)	0.76	0.026		28	1.46		21

Therefore, use of the developed sensor allows to define the diffusion coefficient of ammonia-nitrogen at temperatures up to 400°C.

Finally, the response time of the considered sensor was calculated, by analyzing time dependence (potentiostatic transient) of the limiting current value of the sensor. As it can be observed in Fig. 10.5, this parameter accedes to 3-5min at 400°C, when ammonia content in nitrogen alternates by ~1.5-4 times. Such long period of time from the initial change of a parameter to the final stabilization of a reading is due to slow change of the gas composition in the rather big internal volume of the tubular furnace.

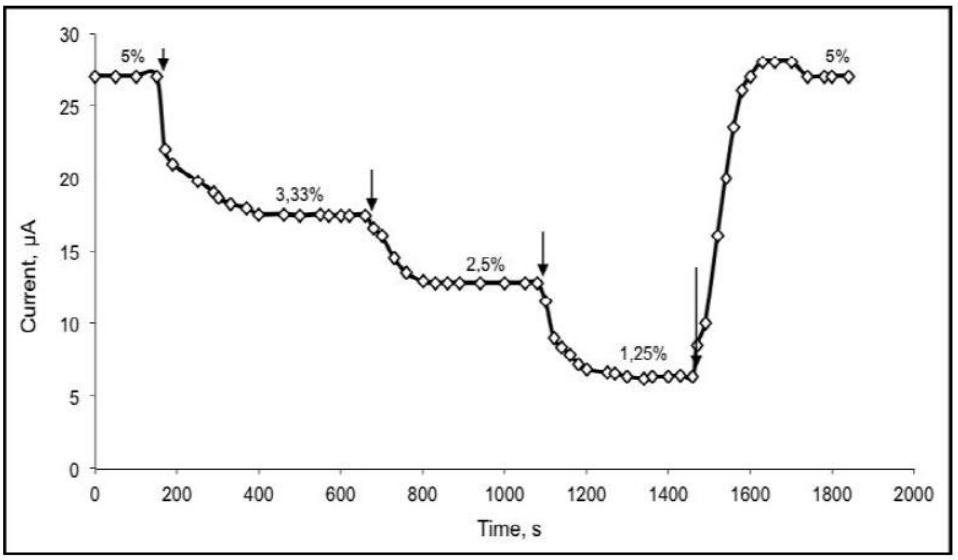

Figure 11.5. Potentiostatic transient: effect of NH_3 concentration on sensor's current by applying a constant voltage of 1.2V at 400°C.

11.5 Conclusions

In the present work a new amperometric sensor was developed, fabricated and investigated. It is used for the measurement of ammonia content in ammonia+nitrogen mixtures. The sensor is based on oxygen ion solid electrolyte and equipped with a diffusion barrier made from chromo-nickel steel. The following conclusions are drawn from the experimental results:

i. The sensor displayed good operating capacity in detecting ammonia in the range of 1-5 vol. % at a temperature range of 375-400^{o}C. It was found that chromo-nickel steel capillary is not applicable as a diffusive barrier for the analysis of the above mixtures at temperatures higher than 400^{o}C due to catalyzing the ammonia decomposition reaction.

ii. The sensor can be used for the estimation of the ammonia's diffusion coefficient in nitrogen, at elevated temperature. The obtained experimental results, on the diffusion coefficients at a temperature of 375-400^{o}C, are in good agreement with the theoretically calculated values. It is possible that the use of materials for the diffusion channel restraining ammonia decomposition will allow acquiring the experimental diffusion coefficient values even at higher temperatures.

iii. The electrochemical oxidation of ammonia on platinum electrodes at 375 and 400^{o}C advances with the formation of molecular nitrogen.

The results presented in this work lead to the conclusion that the as fabricated sensor can be regarded as a useful asset not only for gas analysis but also for estimating the gas diffusion coefficients and occasionally for defining the electrochemical reaction type.

REFERENCES

1. Darrel Ebbing, Steven D. Gammon, *General Chemistry*. 1999.
2. Maria Turco, Angelo Ausiello, and Luca Micoli, *Treatment of Biogas for Feeding High Temperature Fuel Cells*. 2016.
3. Steve Taylor, *Advances in Food and Nutrition Research*. Vol. 61. 2010.
4. Muneeb Irshad, Khurram Siraj, Rizwan Raza, Anwar Ali, Pankaj Tiwari, Bin Zhu, Asia Rafique, Amjad Ali, Muhammad Kaleem Ullah, Arslan Usman, *A Brief Description of High Temperature Solid Oxide Fuel Cell's Operation, Materials, Design, Fabrication Technologies and Performance.* 2015.
5. Deborah S. Gho, Shamsher Singh, *Connection between Ecell , ΔG, and K*. Available from: https://chem.libretexts.org/Core/Analytical_Chemistry/Electrochemistry/Electrochemistry_and_Thermodynamics.
6. *Handbook of Electrochemistry*, C.G. Zoski, Editor. p. 9.
7. John Newmann, Karen Thomas-Alyea, *Electrochemical Systems*. 2004. p. 8.
8. Kazemi Esfeh, M. K. A. Hamid, , *Algebraic Form and New Approximation of Butler–Volmer Equation to Calculate the Activation Overpotential.* 2016.
9. *Verification of Tafel Equation*. Available from: http://vlab.amrita.edu/?sub=2&brch=190&sim=605&cnt=1.
10. *Handbook of Electrochemistry*, C.G. Zoski, Editor. p. 16-17.
11. Rana Afif Majed Anaee, Majid Hameed Abdulmajeed, *Tribocorrosion.*
12. *Handbook of Electrochemistry*, C.G. Zoski, Editor. p. 11.
13. Dominique Piron, *Solved Problems in Electrochemistry for Universities and Industry*. 2004. p. 27.
14. Thomas Drew, *Advances in Chemical Engineering*. p. 213-214.
15. N Zech, Dieter Landolt, *The Influence of Boric Acid and Sulfate Ions on the Hydrogen Formation in Ni–Fe Plating Electrolytes.* 2000.
16. Wilson Rorrer,Wicks Welty, *Fundamentals of Momentum, Heat and Mass Transfer.* 2007.
17. Weidong He, Weiqiang Lv, Dickerson J, *Gas Diffusion Mechanisms and Models*, in *Gas Transport in Solid Oxide Fuel Cells*. 2014.
18. Leonardo Giorgi, Fabio Leccese, *Fuel Cells: Technologies and Applications.* The Open Fuel Cells Journal, 2013.
19. Anatoly Demin, Elena Gorbova, Panagiotis Tsiakaras, *High temperature electrolyzer based on solid oxide co-ionic electrolyte: A theoretical model.* Journal of Power Sources, 2007.
20. Jens Oluf Jensen, Viktor Bandur, Niels J. Bjerrum, Søren Højgaard Jensen, Sune Ebbesen, Mogens Mogensen, Niels Tophøj, Lars Yde, *Pre-Investigation of Water Electrolysis*. 2008.
21. Shijing Wang, Tatsumi Ishihara, *Intermediate Temperature CO2 Electrolysis by Using La0.9Sr0.1Ga0.8Mg0.2O3 Oxide Ion Conductor.* 2014.
22. Miguel A. Guerrero, Enrique Romero, Fermín Barrero, María Isabel Milanés, Eva González, *Supercapacitors: Alternative Energy Storage Systems* Power Electronics & Electric Systems (PE&ES), School of Industrial Engineering (University of Extremadura)
23. Adrian Schneuwly, Roland Gallay, *Properties and applications of supercapacitors from the state-of-the-art to future trends.* 2000.
24. R. Kotz, M. Carlen, *Principles and applications of electrochemical capacitors.* Electrochimica Acta, 2000.
25. Marin S. Halper, James C. Ellenbogen, *Supercapacitors: A Brief Overview.* 2006.

26. Shuai Bana, Jiujun Zhanga, Lei Zhanga, Ken Tsaya, Datong Songa, Xinfu Zoub, *Charging and discharging electrochemical supercapacitors in the presence of both parallel leakage process and electrochemical decomposition of solvent.* Electrochimica Acta, 2012. **90**.
27. Krishnan Rajeshwar, Jorge Ibanez, *Environmental Electrochemistry: Fundamentals and Applications in Pollution Abatement*. 1997.
28. Ole Hammerich, Bernd Speiser, *Organic Electrochemistry: Revised and Expanded*. 5th ed. 2016.
29. Lyle F. Albright, *Albright's Chemical Engineering Handbook*. 2008.
30. Brent Kleven, *A Summary of Gas Detection*.
31. Kousuke Ihokura, Joseph Watson, *The Stannic Oxide Gas Sensor*. 1994.
32. G. Sberveglieri, *Gas Sensors: Principles, Operation and Developments*. 1992.
33. J. Chou, *Hazardous Gas Monitors*. 2000. p. 28-32.
34. Enobong Effiong Bassey, *Development and Characterisation of Metal Oxide Gas Sensors*. 2014, Auckland University of Technology.
35. W. Gopel, G. Reinhardt, M.Rosch, *Trends in the development of solid state amperometric and potentiometric high temperature sensors.* Solid State Ionics, 2000. **136-137**: p. 519-531.
36. R.W. Cattrall, *Chemical Sensors.* Oxford University Press, 1997: p. 80.
37. T. Takeuchi, *Oxygen Sensors.* Sensor and Actuators, 1988. **14**: p. 109-124.
38. *Celox*. Available from: http://www.nksensor.com/ru/proucts/products-materials/105-oxygen-act-system.
39. C. M. Mari, *Non-Nernstian Solid State Gas Sensors: Operating Principles and Materials.* Ionics, 2003. **9**: p. 365-369.
40. G. Fadeyev, A. Kalyakin, E. Gorbova, A. Brouzgou, A. Demin, A. Volkov, P. Tsiakaras, *Electrodes for solid electrolyte sensors for the measurement of CO and H2 content in air.* International Journal of Hydrogen Energy, 2013. **38**: p. 13484-13490.
41. Joffrey W. Fergus, *Sensing mechanism of non-equilibrium solid-electrolyte-based chemical sensors.* Journal of Solid State Electrochemistry, 2011. **15**: p. 971-984.
42. Yixin Liu, Xiangcheng Sun, Yu Lei, Joseph Parisi, *Solid-state gas sensors for high temperature applications – a review.* Journal of Materials Chemistry A, 2014: p. 1-2, 4, 9924-9930.
43. Richard Dorf, *Sensors, Nanoscience, Biomedical Engineering and Instruments*, in *The Electrical Engineering Handbook*. 2006. p. 11.
44. A. Kalyakin, G. Fadeyev, A. Demin, E. Gorbova, A. Brouzgou, A. Volkov, P. Tsiakaras, *Application of solid oxide proton-conducting eletrolytes for amperometric analysis of hydrogen in H2+N2+H2O gas mixtures.* Electrochimica Acta, 2014. **141**.
45. A. Kalyakin, J. Lyagaeva, D. Medvedev, A. Volkov, A. Demin, P. Tsiakaras, *Characterization of proton-conducting electrolyte based onLa0.9Sr0.1YO3 – ıand its application in a hydrogen amperometric sensor.* Sensors and Actuators B: Chemical, 2015.
46. Theodor Doll, *Advanced Gas Sensing: The Electroadsorptive Effect and Related Techniques*. 2003.
47. S. Capone, A. Forleo, L. Francioso, R. Rella, P. Siciliano, J. Spadavecchia, D. S. Presicce,,A. M. Taurino, *SOLID STATE GAS SENSORS: STATE OF THE ART AND FUTURE ACTIVITIES.* Journal of Optoelectronics and Advanced Materials, 2003.
48. Alexander Volkov, Elena Gorbova, Aleksey Vylkov, Dmitry Medvedev, Anatoly Demin, Panagiotis Tsiakaras, *Design and applications of potentiometric sensors based on proton-conducting ceramic materials. A brief review.* Sensors and Actuators B: Chemical, 2017.

49. Dinesh Aswal, Shiv Gupta, *Science and Technology of Chemiresistor Gas Sensors*. 2007. p. 18.
50. A. Kalyakin, A. Volkov, J. Lyagaeva, D. Medvedev, A. Demin, P. Tsiakaras, *Combined amperometric and potentiometric hydrogen sensors basedon BaCe0.7Zr0.1Y0.2O3−proton-conducting ceramic.* Sensors and Actuators B: Chemical, 2016.
51. G. Fadeyev, A. Kalyakin, E. Gorbova, A. Brouzgou, A. Demin, A. Volkov, P. Tsiakaras, *A simple and low-cost amperometric sensor for measuring H2, CO,and CH4.* Sensors and Actuators B: Chemical, 2015.
52. Shunsuke Akasaka, *Thin film YSZ-based limiting current-type oxygen and humiditysensor on thermally oxidized silicon substrates.* Sensors and Actuators B: Chemical, 2016.
53. G. Velasco, J. Ph. Schnell, M. Croset, *Thin solid state electrochemical gas sensors.* Sensors and Actuators B: Chemical, 1982. **2**(YSZ sensor for combustion control): p. 371-384.
54. H. Dietz, *Gas-diffusion-controlled solid-electrolyte oxygen sensors.* Solid State Ionics, 1982. **6**: p. 175-183.
55. Y. Ueda, A. I. Koleshnikov, H. Koyanaka, *Sensoring Hydrogen Gas Concentration Using Electrolyte Made Of Proton Conductive Manganese Dioxide.* Sensors and Actuators B: Chemical, 2011. **155**(Room Temperature): p. 893-896.
56. T. Usui, A. Asada, N. Nakasawa, H. Osanai, *Gas Polarographic Oxygen Sensor Using an Oxygen/Zirconia Electrolyte.* Journal of The Electrochemical Society, 1989. **136**: p. 534-542.
57. T. Usui, Y. Kurumiya, K. Nuri, M. Nakasawa, *Gas-polarographic multifunctional sensor: oxygen-humidity sensor.* Sensors and Actuators, 1989. **16**: p. 345-358.
58. T. Usui, A. Asada, M. Nakasawa, H. Osanai, *Gas polarographic hydrogen sensor using a zirconia electrolyte.* Japanese Journal of Applied Physics, 1989. **28**: p. L1654-L1656.
59. T. Usui, A. Asada, K. Ishibashi, M. Nakasawa, *N2O-gas sensing using a gas polarographic oxygen sensor.* Japanese Journal of Applied Physics, 1989. **28**: p. 2046-2047.
60. T. Usui, A. Asada, K. Ishibashi, M. Nakasawa, *Output characteristics in C2H5OH-N2 gas mixture of a gas polarographic oxygen sensor using a zirconia electrolyte.* Japanese Journal of Applied Physics, 1991. **30**: p. 1496-1497.
61. K. Katahira, H. Matsumoto, H. Iwahara, K. Koide, T. Iwamoto, *A solid electrolyte hydrogen sensor with an electrochemically-supplied hydrogen standard.* Sensors and Actuators B, 2001. **73**: p. 130-134.
62. B. Y. Liaw, Y. Weppner, *Low temperature limiting-current oxygen sensors using tetragonal zirconia as solid electrolytes.* Solid State Ionics, 1990. **40-41**: p. 428-432.
63. Z. Peng, M. Liu, E. Balko, *A new type of amperometric oxygen sensor based on a mixed-conducting composite membrane.* Sensor and Actuators B, 2001. **72**: p. 35-40.
64. Lucjan Chmielarz, Mandalena Jablonska, *Advances in selective catalytic oxidation of ammonia to dinitrogen: a review.* RSC Adv, 2015. **5**: p. 43408-43431.
65. P. G. Ashmore, *Catalysis and inhibition of chemical reactions*. 1963: Butterworth &Co. Ltd.
66. R. C. Reid, J. M. Prausnitz, T. K. Sherwood, *The properties of gases and liquids*. 1977, New York: McGraw-Hill Book Company.